AMERICAN SOCIETY FOR MICROBIOLOGY | Molecular and Cellular Biology

An Outer Mitochondrial Translocase, Tom22, Is Crucial for Inner Mitochondrial Steroidogenic Regulation in Adrenal and Gonadal Tissues

Maheshinie Rajapaksha,[a] Jasmeet Kaur,[a] Manoj Prasad,[a] Kevin J. Pawlak,[a]* Brendan Marshall,[b] Elizabeth W. Perry,[b] Randy M. Whittal,[c] Himangshu S. Bose[a,d]

Department of Biochemistry, Mercer University School of Medicine, Savannah, Georgia, USA[a]; Department of Cellular Biology and Anatomy, Georgia Regents University, Augusta, Georgia, USA[b]; Department of Chemistry, University of Alberta, Edmonton, Alberta, Canada[c]; Anderson Cancer Institute, Memorial University Medical Center, Savannah, Georgia, USA[d]

After cholesterol is transported into the mitochondria of steroidogenic tissues, the first steroid, pregnenolone, is synthesized in adrenal and gonadal tissues to initiate steroid synthesis by catalyzing the conversion of pregnenolone to progesterone, which is mediated by the inner mitochondrial enzyme 3β-hydroxysteroid dehydrogenase 2 (3βHSD2). We report that the mitochondrial translocase Tom22 is essential for metabolic conversion, as its knockdown by small interfering RNA (siRNA) completely ablated progesterone conversion in both steroidogenic mouse Leydig MA-10 and human adrenal NCI cells. Tom22 forms a 500-kDa complex with mitochondrial proteins associated with 3βHSD2. Although the absence of Tom22 did not inhibit mitochondrial import of cytochrome P450scc (cytochrome P450 side chain cleavage enzyme) and aldosterone synthase, it did inhibit 3βHSD2 expression. Electron microscopy showed that Tom22 is localized at the outer mitochondrial membrane (OMM), while 3βHSD2 is localized at the inner mitochondrial space (IMS), where it interacts through a specific region with Tom22 with its C-terminal amino acids and a small amino acid segment of Tom22 exposed to the IMS. Therefore, Tom22 is a critical regulator of steroidogenesis, and thus, it is essential for mammalian survival.

Mitochondrial function is not limited to oxidative phosphorylation, as mitochondria are the site of steroid synthesis in specialized cells. Most mitochondrial proteins are expressed by nuclear genes with the mitochondrial targeting information in the mature protein. For example, some inner mitochondrial matrix (IMM) proteins have an internal, positively charged "presequence"-like signal, often preceded by a hydrophobic sequence (1), which leads to the arrest of translocation in the IMM and the subsequent lateral release of the protein into the lipid phase of the membrane (2). Import and subsequent intramitochondrial sorting of mitochondrial proteins are mediated by the mitochondrial membrane protein translocases. The translocase complexes in the outer mitochondrial membrane (OMM) are not tightly linked with those of the IMM; yet, they dynamically cooperate to achieve protein delivery to each mitochondrial subcompartment. To understand the mechanism of protein transport by the mitochondrial import/sorting system, it is essential to monitor and analyze the dynamic interactions among the constituents of the system.

Steroidogenic cells do not store steroid hormone; therefore, an immediate steroidogenic response requires rapid synthesis of new steroid. Cholesterol mitochondrial transport initiates inner mitochondrial metabolic activity in steroidogenic cells within adrenal and gonadal tissues as well as the brain. Conversion of the first steroid, pregnenolone, to progesterone is catalyzed by 3β-hydroxysteroid dehydrogenase 2 (3βHSD2). Due to its central role in steroidogenesis, changes in 3βHSD2 activity can have a wide range of effects, including hypertension, salt wasting crisis, and impaired sexual development (3–7). We have also identified patients with childhood hypertension and ambiguous genitalia that harbor no mutations in genes involved in the steroidogenic pathways (8). Thus, it is possible that the mitochondrial proteins that regulate 3βHSD2 protein folding play a crucial role in maintaining steroidogenic enzyme activity.

The roles of steroidogenic proteins present in the mitochondria and their mechanism of integration after translocation remain unknown. Most matrix proteins and some inner membrane proteins are synthesized as precursor proteins with an amino-terminal cleavable presequence, which contains a mitochondrial targeting signal. The outer membrane translocator, the TOM40 complex, functions as an entry gate for most mitochondrial proteins. The TOM40 complex is composed of a core complex, consisting of Tom40, Tom22, Tom5, and Tom7, as well as the peripheral receptor subunits, Tom20 and Tom70. The presequence is recognized by another receptor site of the TOM40 complex on the inner mitochondrial space (IMS) side, the *trans* site, which consists of the IMS-facing region of Tom40, Tom22, and Tom7 (9–13). Tom22 is the central receptor of the mitochondrial import channel. In the absence of Tom22, Tom70 and Tom20 can promote import, but the imported proteins are not processed appropriately (14), because Tom22 contacts the inner mitochondrial

Received 22 December 2015 **Accepted** 6 January 2016

Accepted manuscript posted online 19 January 2016

Citation Rajapaksha M, Kaur J, Prasad M, Pawlak KJ, Marshall B, Perry EW, Whittal RM, Bose HS. 2016. An outer mitochondrial translocase, Tom22, is crucial for inner mitochondrial steroidogenic regulation in adrenal and gonadal tissues. Mol Cell Biol 36:1032–1047. doi:10.1128/MCB.01107-15.

Address correspondence to Himangshu S. Bose, bose_hs@mercer.edu.

* Present address: Kevin J. Pawlak, Zirve University, Gaziantep, Turkey.

J.K. and M.P. contributed equally to this work.

hub of the IMS, the sorting and assembly machinery (SAM) complex (15). Thus, in the absence of Tom22, imported proteins are inactive due to misfolding (14). The cytosolic domain of Tom22 mediates protein translocation and import of mitochondrial proteins (15–18), where its negatively charged acid-rich region may interact with the polar surfaces of amphipathic presequences. Tom22 is a C-terminal tail-anchored protein in the mitochondrial outer membrane, and the cytosolic N-terminal domain collaborates with Tom20 to promote protein import (19–23). This led us to hypothesize that the residues present at the IMS side may mediate interaction with steroidogenic enzymes. Most of the amino acids are facing the OMM side of the cytoplast and, thus, are highly flexible. In contrast, the small number of residues exposed through the IMS side are more tightly oriented, requiring a more regulated interaction with the incoming or present metabolic enzymes.

Mitochondrial translocases are present in all species and in all cell types irrespective of their origin, as they are necessary for protein transport and association across the different mitochondrial compartments. Thorough analysis of translocases in *Saccharomyces cerevisiae* and *Caenorhabditis elegans* shows that their mechanism of translocation is similar to that of transport. In steroidogenic cells, in addition to the mitochondrial enzymes, new proteins are transiently expressed during acute stimulation to complete the physiological need, and thus, translocases develop an extra role to work on the transiently expressed proteins for metabolic action. Our results show that 3βHSD2 is associated with Tom22 to regulate metabolic activity. Specifically, the C terminus of Tom22 interacts with 3βHSD2 at the IMS once it enters the mitochondria through its signal sequence present in the amino acid region from amino acids 283 to 310. The unstructured region spanning amino acids 283 to 310 of 3βHSD2 possibly forms a loop for its entry, possibly through Tom40, facilitating the interaction between the C terminus of Tom22 with the C terminus of 3βHSD2.

MATERIALS AND METHODS

Reagents and data analysis. Antibodies against VDAC1, Tom22, and COX IV were obtained from Santa Cruz Biotechnology (Santa Cruz, CA) or AbCam (Cambridge, MA). Antibodies specific for cytochrome P450scc (cytochrome P450 side chain cleavage enzyme) were purchased from ProteinTech (Chicago, IL); rabbit IgG was from Sigma-Aldrich (St. Louis, MO), and protein A beads were from Amersham Pharmacia/GE (Piscataway, NJ). If not otherwise mentioned, all other antibodies were custom synthesized and used in previous studies in our laboratory. RNase A and proteinase K (PK) were from Roche/GE Healthcare (San Francisco, CA); digitonin was obtained from Calbiochem/EMD Biosciences (Billerica, MA). Oligonucleotide primers were obtained from Integrated DNA Technology (Ames, IA). Chemical cross-linkers and small interfering RNA (siRNA) were from Life Sciences (Thermo Fisher, Waltham, MA). All other chemicals were purchased from Sigma-Aldrich, unless otherwise specified. All Western blot experiments were performed three times. Most of the figures are generated from the same experiment, and bands were excised from the same autoradiogram or two different autoradiograms, where the experiments were performed at the same time.

Cell culture, transfection, and animals. Cell culture, transfection, and mitochondrial isolation from cultured cells were performed following our previously described procedure (24). Briefly, the cells were washed with serum-free medium 12 h after transfection and supplemented with medium containing the appropriate antibiotics and 10% serum. In some cases, 100 ng/ml of trilostane (Steraloids, Los Angeles, CA) was added as an inhibitor of 3βHSD2. Mouse Leydig (MA-10) cells were grown in Waymoth medium containing 5% fetal calf serum (FCS) and 10% horse serum supplemented with 1× gentamicin and L-glutamine. COS-1 cells were cultured in Dulbecco's modified Eagle medium (DMEM) with a high level of glucose supplemented with 10% fetal bovine serum (FBS) and penicillin-streptomycin. Mutant Tom22 activity was measured after knocking down Tom22 by siRNA for 24 h followed by transfection of the mutant Tom22 cDNA using Lipofectamine. siRNA transfection was done with 60 pmol of siRNA using Oligofectamine as described previously (25).

Male Sprague-Dawley mice were purchased from Harlan/Sprague-Dawley (Indianapolis, IN). All mice were maintained in a pathogen-free facility. The animal procedure was approved by the institutional review board (IACUC number A1406011) on 8 September 2014. All animals were placed on a standard chow diet (AIN93G; Harlan Teklad Global Diets) for 4 weeks.

Cross-linking. For direct cross-linking and immunoprecipitation experiments, the cells were incubated with 0.3% lauryl maltoside (LM) overnight, washed twice with phosphate-buffered saline (PBS), and processed for mitochondrion isolation as described previously (26), followed by coimmunoprecipitation as described below. For *in vitro* cross-linking, the cells were next incubated with the cross-linker bis(sulfosuccinimidyl)suberate (BS^3) that was added directly to the reaction mixture at a final concentration of 0.3, 0.45, 0.09, 0.15, and 0.45 mM from a stock solution of 50 mM BS^3. The reaction was stopped with 1× sodium dodecyl sulfate (SDS) sample buffer and analyzed by 12.5% or 15% SDS-polyacrylamide gel electrophoresis (PAGE).

Chemical cross-linking. Isolated mitochondrial fractions were incubated with various concentrations of BS^3 solubilized in water, and various concentrations of cross-linkers were added to the mitochondria isolated from MA-10 cells, which were preequilibrated with the appropriate buffer that included LM. The reactions were terminated either by transferring them on ice or by the addition of approximately 10 to 20 μl of 1.0 M Tris buffer, pH 9.0, depending on the experimental requirement. Whole-cell cross-linking was also performed by a major modification of the procedure developed by Selkoe's research group (27). MA-10 cells (5×10^6) grown in tissue culture dishes were washed twice with PBS at room temperature and then collected by gentle scraping. For *in vivo* cross-linking, the cells were next incubated with the BS^3 cross-linker that was added directly to the reaction mixture at a final concentration of 0.1, 2.0. 6.0, and 10.0 mM from a stock solution of 50 mM BS^3. After 1 h of incubation at 37°C in a rotating shaker, the reaction was quenched by the addition of 1 M Tris, pH 7.6, to a final concentration of 50 mM for an additional 15 min at 4°C. To avoid any endogenous protease activity, we immediately added a protease inhibitor cocktail (Pierce, Rockford, IL) for an additional 15 min at room temperature. The cross-linked cells were collected by centrifugation at 3,000 rpm and resuspended in 10 mM HEPES, pH 7.4. Organelle fractionation was performed following a standard procedure previously described (25, 28).

***In vitro* transcription and translation and mitochondrial import.** [^{35}S]methionine (Met)-labeled proteins were translated in a cell-free system (CFS) using a TNT rabbit reticulocyte system (Promega, Madison, WI). Ribosomes and their associated polypeptide chains were removed by centrifugation at 150,000 × *g* for 15 min at 4°C as previously described (29). For all protein import experiments, 100 μg of isolated mitochondria was incubated in a 26°C water bath with ^{35}S-labeled proteins to a final volume of 100 μl, and the reaction was terminated by the addition of 1 mM carbonyl cyanide *m*-chlorophenylhydrazone and an equal volume of boiling 2× SDS sample buffer. For sodium carbonate extractions, after import, the reaction was stopped on ice. The samples were centrifuged at 4°C for 15 min at 10,000 × *g*, and the supernatant and pellet were separated. The pellet containing mitochondria was washed with 100 μl of 1× mixed buffer (28) and centrifuged again for 15 min at 10,000 × *g* at 4°C. For sodium carbonate extractions, the mitochondrial pellet was resuspended in 20 μl of freshly prepared 100 mM Na_2CO_3, incubated for 15 min at 4°C, and again pelleted for 15 min at 13,000 × *g*. The pellet was resuspended with 1× mixed buffer to a final volume of 100 μl, and the

reaction was stopped by 2× SDS buffer. For protease assays, the import reaction mixture was incubated with a range of proteinase K (0.1 to 2 μg/μl) for 15 min at room temperature in the absence and presence of 5% Triton X-100. The reaction was stopped by the addition of 2× SDS buffer followed by boiling in a water bath. The samples were analyzed by SDS-PAGE, fixed in methanol-acetic acid (40:10), dried, and exposed to a phosphorimager screen (digital autoradiography; Molecular Dynamics/GE Healthcare).

Mitochondrial fractionation. The mitochondrial compartments were individually purified following a standard procedure with minor modifications (30, 31). Briefly, the OMM fraction was extracted with 1.2% digitonin, and the remaining mixture of matrix and IMM was in some cases purified through 0.5% lubrol, where the matrix fraction remained in solution after centrifugation and the IMM fraction formed the pellet. The compartment-specific fractions were then processed by Western blotting with specific antibodies.

Immunoprecipitation. Digitonin extracts from mitochondria incubated with MA-10 cells were immunoprecipitated overnight at 4°C with the antibodies in 25 mM Tris-HCl (pH 7.5), 1% Triton X-100, 0.5% NP-40, 200 mM NaCl, 0.5% sodium deoxycholate, 0.01 to 0.03% SDS, and 1× protease inhibitor cocktail. Preimmune serum, IgG, or goat serum was added for a negative control, and 3βHSD2 antiserum was added for a positive control. Protein A–Sepharose CL-4B (GE Healthcare/Amersham Biosciences) was used to isolate the immunocomplexes, which were eluted by boiling for 15 min in 1× SDS sample buffer and analyzed by SDS-PAGE.

Density gradient ultracentrifugation. Complexes were resolved by a sucrose density gradient (10% [top] to 30% [bottom]) with a cushion of 200 μl of 68% (2.0 M) sucrose to a final volume of 2 ml. Approximately 100 μg of protein in 100 μl was layered on the top and centrifuged at 4°C in a Beckman TLA55 rotor at 55,000 rpm for 4 h. After centrifugation, fractions of 125 μl were collected. Gradient fractions were analyzed by SDS-PAGE to confirm that the complexes were not degraded during the sucrose density gradient resolution. An aliquot of 20 μl of each fraction was analyzed via 15% SDS-PAGE; the same volume was processed for immunoprecipitation and Western blot analyses.

siRNA knockdown and metabolic conversion. We used the same sequence for knocking down Tom22 as previously described (25). To knockdown VDAC2 expression, MA-10 or COS-1 cells were incubated with 30 or 60 pmol siRNA (sense, 5′-GGUUAGCCUACUCUCUAAUT T-3′; antisense, 5′-AUUAGAGAGUAGGCUAACCTT-3′) for 24, 36, and 48 h after which target protein expression was determined by Western blotting with specific antibodies. Conditions that yielded at least 80% knockdown were used for subsequent analyses. For studies in which mutant Tom22 was overexpressed, wild-type Tom22 was first knocked down with siRNA using Oligofectamine (Thermo Fisher) for 15 h. The cells were washed with serum-free media, and mutant Tom22 cDNA was transfected following our procedure using Lipofectamine (31). The cells were collected after 36 h. For metabolic conversion, 20 μg of mitochondrial protein or cell lysate was incubated with NAD for evaluation of the conversion of pregnenolone to progesterone. For quantitative analysis of each steroid synthesized, radioactive spots on the silica plates were scraped off, and the silica was extracted with a solvent mixture of ether-chloroform (3:1). After the solvent was evaporated under N_2, the extract was resuspended in 100 μl methanol (MeOH), and radioactive counts were determined. The endogenous progesterone activity was determined (25, 32), and the steroids were characterized by gas chromatography and mass spectrometry (33).

3βHSD2 mRNA expression in the ΔTom22 MA-10 cells was analyzed by RT-PCR analysis. Briefly, after Tom22 knockdown in MA-10 cells by siRNA, total RNA was isolated using TRIzol following the manufacturer's protocol (Life Technology, Carlsbad, CA). Then, 500 ng of total RNA was incubated with various combinations of forward and reverse gene-specific primers for PCR amplification using SuperScript one-step reverse transcription-PCR (RT-PCR) with Platinum Taq following the manufacturer's protocol (Life Technology, Carlsbad, CA). The primer combinations were as follows: sense KJP23 (5′-AGCTGGATCCATGGG CTGGAGCTGCCTTGTGACA-3′) and antisense MP354 (5′-TGCTACC GGTGTAGATGAAGACTGGCA-3′) (369 bp), sense MP355 (5′-TACA CCGGTAGCATAGAGGTAGCCGG-3′) and antisense JT2 (5′-AGCT GAATTCTCACTGAGTCTTGGACTT-3′) (747 bp), sense KJP23 and antisense MP356 (5′-TTGTAGCCGTTGGGCCCGGCTACCTC-3′) (396 bp), and sense KJP23 and antisense MP358 (5′-TTATACCGGC AGAAAGGAATGGGC-3′) (600 bp). The 3βHSD2 plasmid cDNA was used as a control for amplification and was amplified independently.

Mitoplast isolation and mitochondrial fractionation. After the import assays, mitochondria were pelleted by centrifugation at 10,000 × *g*. Mitoplasts were prepared by solubilizing OMM in 1.2% (wt/vol) digitonin. Prior to digitonin treatment, mitochondria were incubated with 10 mM HEPES (pH 7.4) for 5 min. After digitonin treatment, mitochondria were centrifuged at 10,000 × *g* for 20 min to separate the OMM from the IMM and matrix (mitoplast). IMM and matrix fractions were prepared by the treatment of mitoplasts with nonionic lubrol (0.16 mg/mg of mitochondria), followed by ultracentrifugation at 130,000 × *g* for 1 h. The soluble fraction was referred to as the matrix, and the insoluble part was referred to as the IMM. The matrix fraction (supernatant) was removed, and the membrane pellet was resuspended in 1:1 mix buffer and kept on ice. The volume of the supernatant was measured, and the membrane pellet was resuspended in 1:1 mix buffer.

Mass spectrometry. Following SDS-PAGE or native gradient PAGE, the stained protein bands were excised from the gel. The selected bands were reduced with dithiothreitol (DTT) (Roche, San Francisco, CA) and then alkylated with iodoacetamide (Sigma). Excess alkylating reagent was removed, and the excised gel bands were dried. Sequencing-grade modified trypsin (Promega) was added, and digestion was allowed to take place overnight (34). The resulting peptides extracted from the gel were analyzed by liquid chromatography followed by tandem mass spectrometry (LC MS/MS) on a nanoAcquity ultraperformance liquid chromatograph (UPLC) (Waters, MA) coupled with a quadrupole time of flight (Q-TOF) Premier mass spectrometer (Waters, MA). The tryptic peptides were separated using a linear water/acetonitrile gradient containing 0.1% formic acid. The peptides were initially desalted on a Waters Symmetry column (5-μm C_{18}, 180-μm inner diameter [ID] by 20 mm) coupled directly to a Waters nanoAcquity column (3-μm Atlantis dC_{18}, 100-Å pore size, 75 μm ID by 15 cm). Peak lists were generated using Waters ProteinLynx Global Server software (version 2.2.5). Protein identification was completed by submitting the peak lists to Mascot MS/MS Ion Search at www.matrixscience.com (Matrix Science, United Kingdom), searching the NCBI nonredundant database with consideration for carbamidome thylated cysteine and oxidation of methionine.

For characterization of the steroids identified by thin-layer chromatography (TLC), the spots extracted from TLC plates were subjected to gas chromatography-mass spectrometry (GC-MS) analysis on an Agilent 7890 GC with a 5975C mass spectrometer. The column used was a Phenomenex Zebron ZB-5MS column (30 m; 0.25-mm ID) with a 0.25-μm film thickness. Samples were dissolved in 50 μl of dichloromethane, and 1 μl was injected onto the column using a pulsed splitless injection. Helium was used as the carrier gas at a flow rate of 1 ml/min. The temperature program was as follows: 50°C (hold for 2 min) and then ramp at 10°C/min to 290°C (hold for 4 min). Spectra were collected in full scan mode with 70-eV ionization over the mass range *m/z* 30 to 500 to facilitate the comparison of the MS spectra with the NIST/EPA/NIH NIST08 mass spectral library. For quantitative analysis of each steroid synthesized, radioactive spots on the silica plates were scraped off, and the silica was extracted with a solvent mixture of ether-chloroform (3:1). After the solvent was evaporated under N_2, the extract was brought up in 100 μl of MeOH, and the radioactive counts were determined.

Electron microscopy. To analyze the localization of 3βHSD2 and Tom22 in the mitochondria of both the steroidogenic MA-10 and nonsteroidogenic COS-1 cells, electron microscopy (EM) experiments were

performed. The cells (6×10^6 MA-10 cells and 9×10^6 COS-1 cells) were washed twice with PBS, gently scraped off the plates in the presence of PBS, and transferred to 50-ml plastic disposable Corning tubes. After centrifugation at 3,500 rpm (Beckman Allegra 22R and rotor F630) for 10 min, the cells were fixed in 4% formaldehyde and 0.2% glutaraldehyde in 0.1 M sodium cacodylate buffer (pH 7.4), dehydrated with a graded ethanol series through 95%, and embedded in LR White resin. Thin sections of 75-nm thickness were cut with a diamond knife on a Leica EM UC6 ultramicrotome (Leica Microsystems, Bannockburn, IL) and collected on 200-mesh nickel grids. The sections were first blocked in 0.1% bovine serum albumin (BSA) in PBS for 4 h at room temperature in a humidified atmosphere followed by incubation with a 1:50 dilution of Tom22 in 0.1% BSA overnight at 4°C. The sections were washed five times with PBS and floated on drops of anti-primary specific ultrasmall (<1.0-nm) Nanogold reagent (Nanoprobes, Yaphank, NY) diluted 1:2,000 in 0.1% BSA in PBS for 2 to 4 h at room temperature. After five washes with PBS and five washes with deionized H_2O, the sections were incubated with HQ Silver (Nanoprobes, Yaphank, NY) for 8 min for silver enhancement, followed by washing in deionized H_2O. For double immunolabeling, the same sections were first labeled with a Tom22 antibody (1:2,000), followed by incubation with a 1:2,000 dilution of anti-3βHSD2 (1:2,000) overnight at 4°C, resulting in silver enhancement of the gold particles labeling Tom22 for twice as long as the gold particles labeling 3βHSD2 and therefore producing two different sizes of gold particles. After a final washing, grids were stained with 2% uranyl acetate in 70% ethanol to increase the contrast. The grids were washed an additional five times with deionized H_2O and air dried. The large gold particles were an average of 55 nm in diameter with 90% of the gold particles being between 45 and 65 nm in diameter. The small gold particles were an average size of 15 nm with 90% of the gold particles being smaller than 25 nm in diameter. The cells were observed using a JEM 1230 transmission electron microscope (JEOL USA Inc., Peabody, MA) at 110 kV and imaged with an UltraScan 4000 charge-coupled-device (CCD) camera and First Light digital camera controller (Gatan Inc., Pleasanton, CA). Twenty sections from each experiment were analyzed.

Figure preparation. The data were obtained from the autoradiogram or from scanning with a phosphorimager. Some figures were generated by selecting specific lanes either from the same autoradiogram or from two parallel experiments performed at the same time.

RESULTS

3βHSD2 amino and carboxyl termini are strongly conserved. The minimum length of a mitochondrial leader sequence is 15 amino acids (35); however, proteins targeted to the endoplasmic reticulum (ER) may have pause sequences that reside within the leader sequence or may follow the leader sequence with variable lengths of up to 60 amino acids (36, 37). As shown in Fig. 1A (top panel), comparison of the first 73 amino acids of the 3βHSD2 sequence in seven mammals revealed extreme similarity in the sequences. The N-terminal targeting 15-amino-acid sequence has 100% homology with the exception of the orangutan, rat, mouse, and golden bamboo lemur, which has one extra methionine at the N terminus. In addition, comparison of the carboxyl-terminal 84 amino acids showed 100% amino acid identity with the exception of 8 amino acids that were different in golden bamboo lemur (Fig. 1A, bottom panel), suggesting that the protein is conserved across species. Computational analysis of these amino acid sequences, which include the leader sequence, shows a potentially flexible amphiphilic helix containing a large number of positively charged amino acids, which resembles other mitochondrial leader sequences (38).

Steroidogenic cells express 3βHSD2 in specific tissues for immediate metabolic activity. However, the mechanism of 3βHSD2 import into the mitochondria and necessity of specific translocases for targeting it into the specific compartment is not understood. Sensitivity to proteolysis can be used to assess the topology of a protein; full protection from an exogenous protease can indicate the complete translocation of a protein to a specific mitochondrial compartment. Conversely, digestion of certain domains to yield discrete protease-protected fragments indicates a membrane-spanning topology given that the topology assay is performed in the presence of detergent. As shown in Fig. 1B, 3βHSD2 was resistant to proteolysis with proteinase K (PK) even at concentrations of 1.0 μg/ml; however, the addition of 0.25% detergent with PK induced proteolysis, suggesting that the protein conformation is not tightly folded (24). The addition of detergent did not facilitate 3βHSD2 proteolysis with lower concentrations of protease, as the detergent micelles protected it (Fig. 1B) (39). Mitochondrial fractionation of ^{35}S-3βHSD2 followed by proteolysis with PK showed that the size of the imported 3βHSD2 was similar to that of the full-length unimported protein primarily present at the IMM, confirming that it was imported without cleavage of its N terminus or signal sequence (Fig. 1C).

To understand how 3βHSD2 mitochondrial targeting is regulated by its signal sequence, we created fusion proteins in which the 22-amino-acid N-terminal signal sequence of the mitochondrial matrix-resident COX IV was fused with full-length 3βHSD2 generating the 1-22 COX IV-3βHSD2 [(1-22) COX IV+ (1-372) 3βHSD2] fusion protein, as this region is sufficient for mitochondrial targeting (40). Cell-free synthesis of chimeric 1-22 COX IV-3βHSD2 in a rabbit reticulocyte lysate system labeled with [^{35}S]methionine followed by import into the isolated mitochondria resulted in a protein whose size was similar to the unimported protein size due to noncleavage of the fusion protein (Fig. 1D). Also, the imported fraction remained in the pellet even after extraction with sodium carbonate, which interferes with protein-protein but not lipid-protein interactions, suggesting that the fusion construct was imported into the mitochondria (Fig. 1D, bottom). However, similar analysis with ^{35}S-(1-22) COX IV + (1-224) DHFR, a chimera of the first 22 amino acids of COX IV with the full-length dihydrofolate reductase (DHFR), showed signal sequence cleavage following mitochondrial import (Fig. 1D). Because DHFR is a soluble cytosolic protein, it remained in the supernatant following carbonate extraction.

To evaluate whether a longer sequence of COX IV could impact 3βHSD2 mitochondrial import, we created an additional fusion protein, (1-50) COX IV-3βHSD2. Analysis of ^{35}S-(1-50) COX IV-3βHSD2 following import into isolated mitochondria revealed that the chimeric protein was still not cleaved (Fig. 1E); however, the cleavage was generated from (1-50) COX IV-DHFR as expected (Fig. 1E). This experiment suggests that 3βHSD2 import occurs through a mechanism independent of mitochondrial cleavage in which the 3βHSD2 sequence changed the folding of the fusion protein in such a fashion that the mitochondrial cleavage mechanism is changed. To confirm the accuracy of the experiment, we overexpressed (1-22) COX IV-DHFR in COS-1 cells in the absence or presence of methotrexate (MTX), a DHFR inhibitor. As shown in Fig. 1F, only the high-molecular-weight band was observed with MTX, confirming the absence of mitochondrial import. Taken together, these data suggest that the 3βHSD2 conformation simply covers the cleavage site, and thus, the passenger sequence regulates mitochondrial cleavage.

We next determined whether the N-terminal modification of

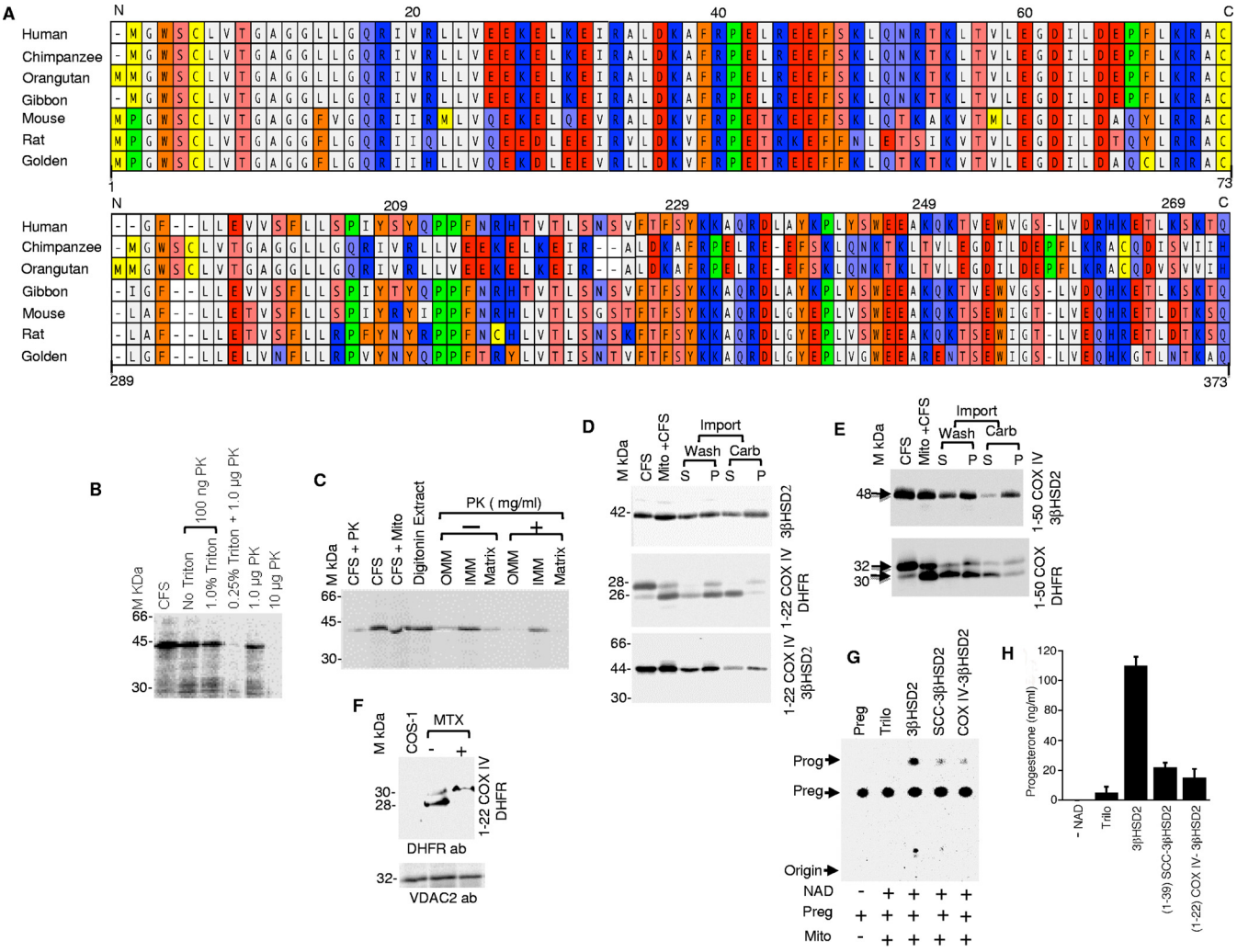

FIG 1 3βHSD2 requires an accessible N terminus for cleavage-independent mitochondrial import. (A) The N-terminal 73-amino-acid and C-terminal 84-amino-acid sequences of 3βHSD2 were compared in seven different species, revealing that they are highly conserved. (B) [^{35}S]methionine-labeled 3βHSD2 was synthesized in a cell-free system, and its folding was analyzed in the presence and absence of different concentrations of nonionic detergents and proteinase K (PK) following import into mitochondria isolated from MA-10 cells. The positions of molecular mass markers (M) are indicated to the left of the gel. (C) Analysis of ^{35}S-3βHSD2 import into the mitochondrial fraction followed by PK digestion of the outer mitochondrial membrane (OMM), intermitochondrial membrane (IMM), and matrix. (D) Mitochondrial import of 3βHSD2, (1-22) COX IV-DHFR, and (1-22) COX IV-3βHSD2. Mito, mitochondria; CFS, cell-free transcription/translation system; Carb, washing with sodium carbonate; S, supernatant; P, pellet. (E) 3βHSD2 determines the N-terminal cleavage pattern. Import of the N-terminal 50 amino acids of COX IV fused with either 3βHSD2 or DHFR into isolated mitochondria. The imported fraction was separated from the unimported fraction, and membrane integration was assessed by sodium carbonate extraction. (F) Overexpression of (1-22) COX IV-DHFR in COS-1 cells in the presence (+) and absence (−) of methotrexate (MTX), followed by identification by Western blotting with a DHFR antibody (ab). The bottom panel shows equivalent loads after staining with a VDAC2 antibody. (G) The metabolic activity of the wild-type 3βHSD2 and chimeric 3βHSD2 cDNA fused with COX IV or 39 amino acids of cytochrome P450scc (SCC) was determined in COS-1 cells expressing the F2 fusion vector. Prog, progesterone; Preg, pregnenolone; Trilo, trilostane. (H) Quantitative measurement of the synthesized progesterone. Data represent means plus standard errors of the means (SEM) (error bars) for three independent experiments performed at three different times.

3βHDS2 impacts its folding and possibly metabolic activity as was observed with a chimera consisting of the steroidogenic protein StAR (steroidogenic acute regulatory protein) fused with Tom20 (N-Tom20-StAR-C) that demonstrated a twofold increase in activity (24). Analysis of progesterone synthesis in COS-1 cells accompanied with the F2 vector, which expresses the complete P450scc system, including the side chain cleavage enzyme fused with ferredoxin and ferredoxin reductase as a single fusion protein (41), revealed more than a 10-fold reduction with the (1-22) COX IV-3βHSD2 fusion compared to wild-type (WT) 3βHSD2 (Fig. 1G and H). Furthermore, a drastic reduction in progesterone levels was also observed with the (1-39) SCC-3βHSD2 fusion protein (SCC is the side chain cleavage enzyme), suggesting that the conformation of 3βHSD2 is tightly regulated for metabolic activity at the IMS (Fig. 1G and H).

Mitochondrial import of 3βHSD2 requires amino acids 283 to 310. To understand the specific amino acids necessary for 3βHSD2 mitochondrial import, we analyzed our previously developed model structure and observed that amino acids 283 to 310 are exposed to the membrane (42, 43). The space-filling model (42, 43) shows that this particular region is unstructured and, thus, possibly requires association with the membrane for stabili-

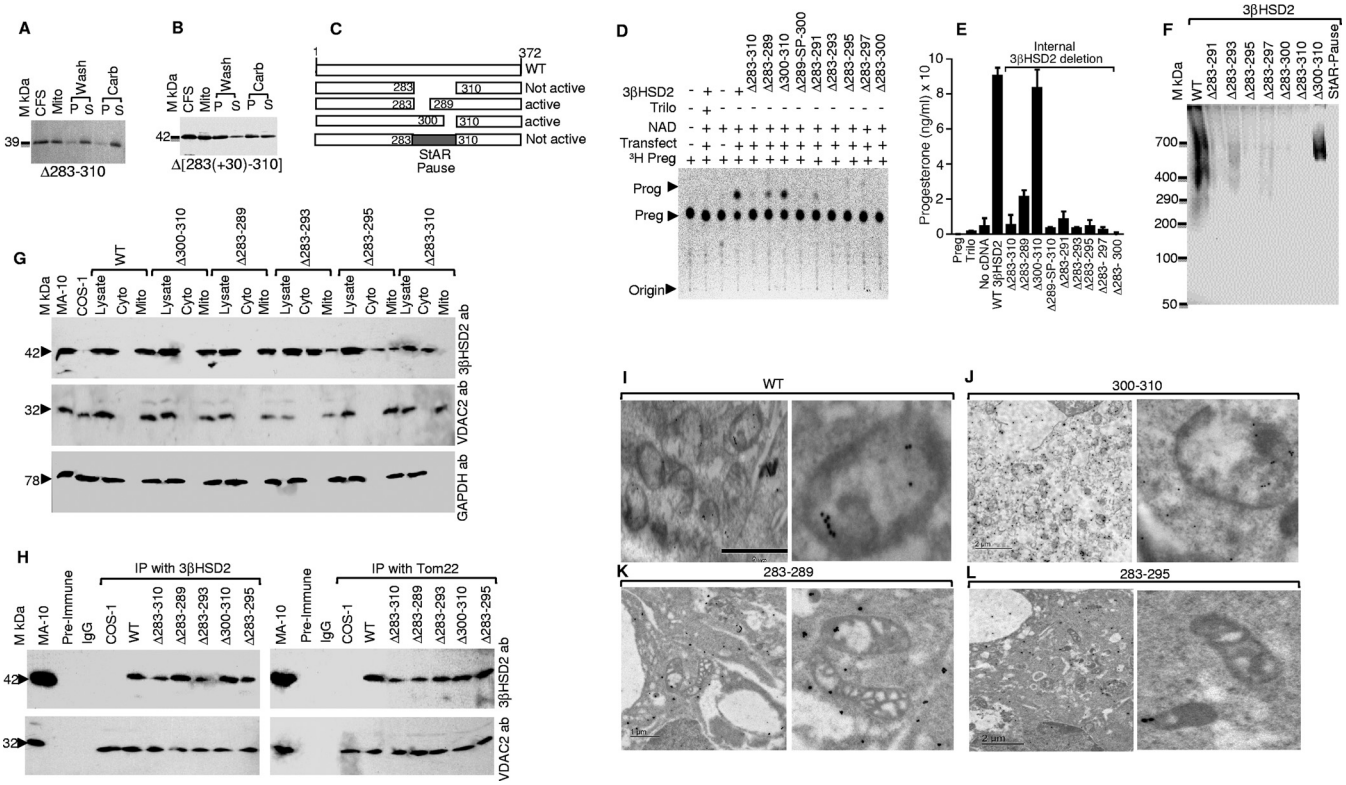

FIG 2 Role of amino acids 283 to 310 in mitochondrial import of 3βHSD2. (A) Analysis of ^{35}S-Δ283-310 3βHSD2 import into the isolated mitochondria and identification of compartmentalization by centrifugation followed by washing with sodium carbonate. (B) Replacement of amino acids 283 to 310 with the 30-amino-acid StAR pause sequence in 3βHSD2 and analysis of its import into isolated mitochondria as in panel A. (C) Schematic presentation of the different internal amino acids from positions 283 to 310 and also substitution of the sequence of the StAR pause sequence from 31 to 61 amino acids. (D) Analysis of the metabolic activity of the indicated 3βHSD2 deletion mutants after cotransfection of COS-1 cells with the F2 vector. Transfect, transfection. (E) Quantitative measurement of the amount of progesterone synthesized in panel D. Data represent the means plus SEM for three independent experiments performed at three different times. (F) Identification of 3βHSD2 mutant-containing complexes after cell-free synthesized ^{35}S-3βHSD2 was imported into mitochondria isolated from MA-10 cells, solubilized with digitonin, and analyzed by 6 to 16% native gradient PAGE. (G) Compartment-specific localization of WT and mutant 3βHSD2 after overexpression in COS-1 cells followed by staining with a 3βHSD2 antibody. The fractions are mitochondria (Mito) and cytoplasm without lipids (Cyto). The middle and bottom panels show a representative Western blot of the same membrane probed with a mitochondrial VDAC2 antibody and a cytosolic glyceraldehyde-3-phosphate dehydrogenase (GAPDH) antibody, respectively. (H) Immunoprecipitation of the 3βHSD2 constructs obtained from COS-1 cells in mitochondrial extracts with 3βHSD2 (left) and Tom22 (right) followed by Western blotting with a 3βHSD2 (top) and VDAC2 (Bottom) antibodies. (I to L) Electron microscopic analysis of WT 3βHSD2 (I), 300-310 3βHSD2 (J), 283-289 3βHSD2 (K) and 283-295 3βHSD2 (L). The right panels show an enlarged view of a mitochondrion from the respective left panels. Bars, 0.5 μm (I), 1.0 μm (K), and 2.0 μm (J and L).

zation. However, this region was completely protected from proteolysis with trypsin even in the presence of lipid vesicles or chemical chaperones (42, 43), suggesting that it might play a crucial role in its metabolic activity. Therefore, we assessed the requirement of this region for 3βHSD2 mitochondrial import in MA-10 cells. As shown in Fig. 2A, mitochondrial fractionation revealed that most ^{35}S-Δ283-310 3βHSD2 was present in the supernatant fraction, indicating that it was not imported into the mitochondria. Replacing this 27-amino-acid region with the well-established mitochondrial pause sequence of StAR that spans amino acids 31 to 62 (24) revealed that the majority of ^{35}S-Δ283(+30)-310 3βHSD2 remained in the pellet and, thus, was imported into the mitochondria (Fig. 2B). Following sodium carbonate extraction, 50% remained in the pellet (Fig. 2B), confirming that the chimeric protein was imported into the mitochondria to a level similar to that of WT 3βHSD2.

We next analyzed whether this specific region has any role in metabolic activity in COS-1 cells cotransfected with F2 using various deletion constructs as presented in the scheme (Fig. 2C). The deletion of amino acids 283 to 310 (Fig. 2D and E) dramatically reduced progesterone levels, and activity was fully restored with the Δ300-310 3βHSD2 protein, which was similar to WT 3βHSD2. Furthermore, substitution of the StAR pause sequence at amino acids 283 to 310 also did not restore activity (Fig. 2D and E), but minimal activity was detected with the 283-289 deletion mutant, suggesting that amino acids 290 to 300 are most crucial for progesterone synthesis. To analyze the requirement of amino acids 283 to 300 for interaction with the mitochondrial membrane, we imported [^{35}S]methionine-labeled cell-free synthesized WT and mutant 3βHSD2 into mitochondria isolated from MA-10 cells. Next, we isolated the ^{35}S-labeled import complex solubilized with digitonin and performed native gradient PAGE analysis. As shown in Fig. 2F, a complex was formed with WT 3βHSD2 and Δ300-310 3βHSD2 mutant with a very minimal complex observed with the 283-289 3βHSD2 mutant. To confirm that the complex formation is associated with mitochondrial import and specificity of the Δ283-310 deletion mutant, we overexpressed the mutants in COS-1 cells, isolated the mitochondrial fractions, and

performed Western blot analysis with 3βHSD2 antibody (Fig. 2G). WT protein and Δ300-310 and Δ283-289 3βHSD2 mutant proteins were detected in the mitochondrial fraction (Fig. 2G). For a control, we also probed the same membrane with antibodies specific for the OMM-associated protein, VDAC2 (Fig. 2G), and cytosolic glyceraldehyde-3-phosphate dehydrogenase (GAPDH) (Fig. 2G), validating the accuracy of the organelle separation. To understand the degree of interaction of the deletional mutants with the mitochondrial membrane, we expressed the indicated mutants in COS-1 cells, isolated their mitochondria, and performed immunoprecipitation (IP) analysis using 3βHSD2 (Fig. 2H, left panels) and Tom22 (Fig. 2H, right panels) antibodies and then stained with 3βHSD2 antibody (Fig. 2H, top panels). The signal obtained with the Δ300-310 and Δ283-289 mutants was similar to that observed with the WT (Fig. 2H). As expected, immunoelectron microscopic analysis showed that the Δ283-289 mutant was evenly distributed (Fig. 2K), but Δ283-295 and more deletional mutants were mostly located outside the mitochondria (Fig. 2L); however, WT and Δ300-310 3βHSD2 were localized within the mitochondria (Fig. 2I and J). The sequence may be acting as an alternate pause, where the region from amino acids 283 to 289 is the first pause and the region from amino acids 287 to 300 is the mandatory sequence on the mitochondrial membrane. In summary, within the region spanning amino acids 283 to 310, only the amino acids from positions 283 to 300 are necessary for 3βHSD2 activity and essential for pausing at the OMM and facilitating 3βHDS2 mitochondrial import.

Establishing the role of a mitochondrial translocase in regulating 3βHSD2 activity. To understand the potential role of mitochondrial membrane proteins in regulating 3βHSD2 activity, ^{35}S-3βHSD2 was imported into mitochondria isolated from MA-10 cells and then solubilized with various concentrations of lauryl maltoside (LM) followed by native gradient PAGE. In the presence of 0.5% LM, the complex size was approximately 500 kDa, and the intensity was reduced or absent with 0.75% and 1.0% LM, respectively (Fig. 3A). The solubilization with LM remained proportional or similar when analyzed by SDS-PAGE and identified by staining with 3βHSD2 and VDAC2 antibodies independently (Fig. 3A). To determine the integrity of the complex, we excised the complex formed with 0.5% LM and subjected it to two-dimensional (2D) native PAGE (Fig. 3B). The continued integrity of the complex suggests that LM may have formed smaller spherical micelles (a monodisperse population, with a polydiversity index [PDI] of <0.1), preserving the conformation longer (44–46).

To assess the metabolic activity associated with this complex, mitochondria were isolated from MA-10 cells after incubating with various concentrations of LM for 36 h. Activity was compared with the LM-treated and untreated mitochondria isolated from the cells maintained under identical conditions (details in Materials and Methods). As shown in Fig. 3C and D, treatment with 0.5% LM showed 80 ng of pregnenolone compared to the 16 ng obtained with the untreated mitochondria. The amount of pregnenolone was measured per milliliter of reaction mixture performed with 20 μg of mitochondria. Thus, LM-incubated mitochondria were five times more active than untreated mitochondria (Fig. 3C). The pregnenolone-to-progesterone reaction is processed through a keto-enol tautomerism, which always remains in equilibrium. It is possible that the keto-enol tautomerism is facilitated by the smaller micelles of LM, favoring metabolic conversion and resulting in increased progesterone synthesis.

We next excised the LM-solubilized complex and subjected it to mass spectrometric analysis to identify the proteins within the complex in the native gradient PAGE as well as the 2D native gradient PAGE. As shown in Tables 1 and 2, mitochondrial proteins, including 3βHSD2 and Tom22, were identified. With the exception of Tom22 and 3βHSD2, the other mitochondrial proteins analyzed are the mitochondrial enzymes responsible for mitochondrial enzymatic activity (Tables 1 and 2). Tom22 is an OMM-integrated protein whose C terminus extends to the IMS (47). To understand the role of Tom22 in the metabolic activity of steroidogenic cells, we knocked down Tom22 expression in steroidogenic MA-10 cells with 60 pmol of siRNA, resulting in a 90% reduction in Tom22 expression but not COX-IV or VDAC2 (Fig. 3E). To confirm that the Tom22 C-terminal mutants (K141D and N124K) were indeed localized at the OMM after siRNA knockdown, we separated the OMM fraction (Fig. 3F, O lanes) from the IMM (Fig. 3F, I lanes) and matrix fragment and stained with 3βHSD2 and Tom22 antibodies independently. 3βHSD2 expression was greatly decreased following Tom22 knockdown (Fig. 3F, top panel). As expected, the Tom22 mutants were present at the OMM (O lanes) at a level similar to that observed in WT cells (Fig. 3F). Probing the same membrane with VDAC2 antibodies showed the same level of expression in the OMM fraction (Fig. 3F), confirming the accuracy of our separation procedure. Because Tom22 is crucial for mitochondrial protein translocation, we first wanted to confirm that reducing its expression did not alter mitochondrial physiology as a whole. As shown in Fig. 3G, the absence of Tom22 did not impact the expression of the matrix-resident aldosterone synthase (AS) or SCC (Fig. 3G); however, 3βHSD2 expression was reduced (Fig. 3H). Furthermore, Tom22 knockdown reduced the synthesis of progesterone from 110 to 33 ng/ml (Fig. 3I). As shown in Fig. 3J, our human 3βHSD2 antibody recognized only the 3βHSD2 protein but not the 3βHSD1 protein, whereas commercial antibody recognized both (Fig. 3J), confirming the accuracy of 3βHSD2 expression and translocation experiments. Our multiple attempts to establish cells with reverse knockdown of 3βHSD2 by siRNA were lethal in both MA-10 cells and human adrenal NCI H295 cells. Taken together, these data suggest that Tom22 is essential for 3βHSD2 metabolic activity in steroidogenic cells.

Analysis of 3βHSD2 and Tom22 localization by electron microscopy. We next analyzed the specific localization of 3βHSD2 and Tom22 in mitochondria using immunoelectron microscopy using our antibody that is specific for 3βHSD2 (Fig. 3J) in combination with a Tom22 antibody. As shown in Fig. 4A, 3βHSD2 was localized to mitochondria, and an enlarged view showed that the protein is specifically localized at the OMM and also within cristae of the IMS but not in the free mitochondrial space or the matrix (Fig. 4B). However, Tom22 was localized only at the OMM (Fig. 4C), which was confirmed at a higher magnification (Fig. 4D). A computational analysis of Tom22 distribution in 40 mitochondria from 20 randomly selected grids showed 180 Tom22 gold labels at the OMM and 16 others at nonspecific positions. Similar analysis of 3βHSD2 distribution showed 450 gold labels at the mitochondria, of which 56 labels were at the IMM. For colocalization analyses, we used 15-nm gold particles for 3βHSD2 and 55-nm gold particles for Tom22 (48). Probing with both antibodies simultaneously showed that Tom22 is localized only at

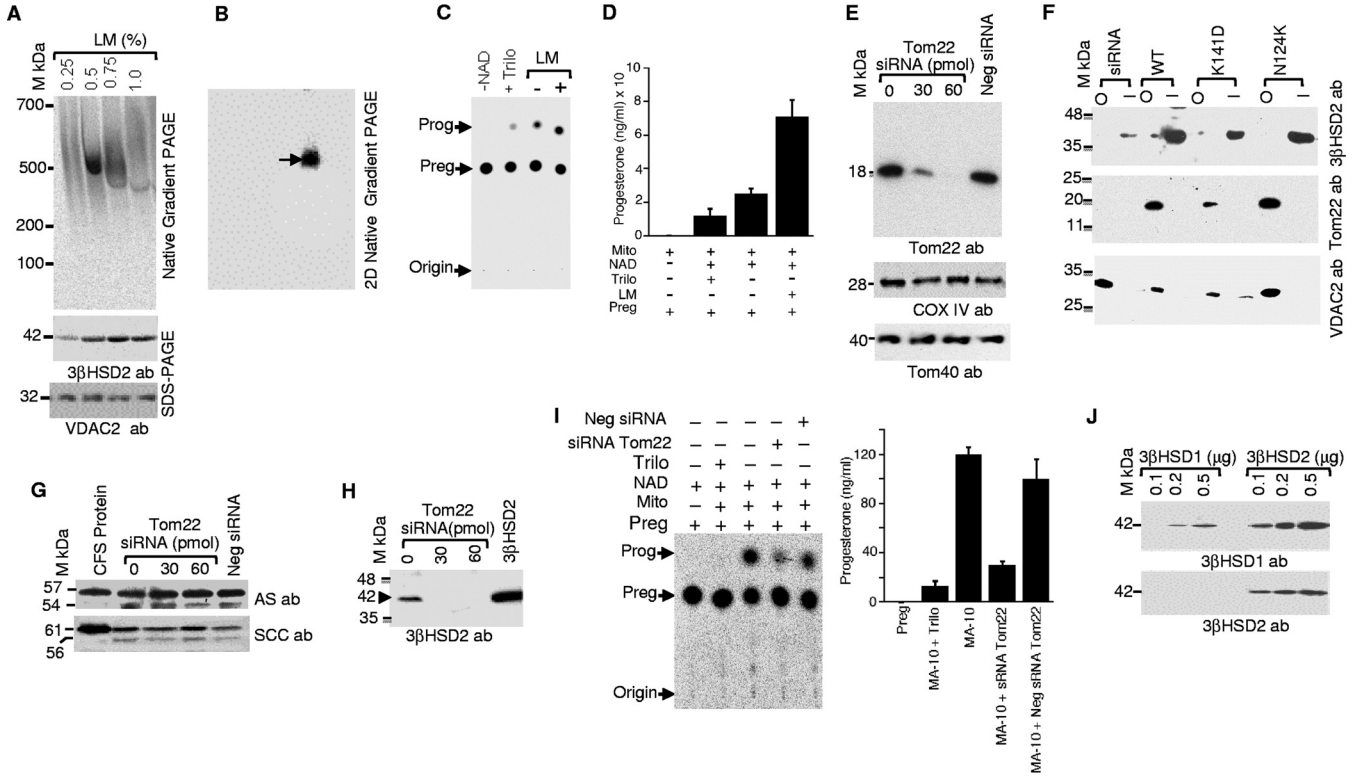

FIG 3 Analysis of the 3βHSD2-containing mitochondrial translocase complex. (A and B) ^{35}S-3βHSD2 was imported into isolated mitochondria and then solubilized with various concentrations of lauryl maltoside (LM) after which the complex was analyzed through 4 to 16% native gradient PAGE (A). (Bottom) The equivalent loads of the relative LM-solubilized fractions were analyzed by SDS-PAGE, followed by Western blot staining with 3βHSD2 and VDAC2 antibodies. The complex formed with 0.5% LM was excised from the 1D native PAGE and analyzed through 2nd dimension native gradient PAGE under identical conditions (B). (C) Metabolic conversion assays of mouse adrenal tissues preequilibrated with 0.5% LM overnight and then the coactivator, NAD, and [^{3}H]pregnenolone. The accumulated progesterone was identified by thin-layer chromatography. (D) Quantitative measurement of the progesterone synthesized in panel C. (E) Expression of Tom22 after knockdown with two different concentrations of negative siRNA. (F) Expression and localization of 3βHSD2 within the mitochondria in ΔTom22 MA-10 cells. 3βHSD2 (top) and Tom22 (middle) expression was absent in the outer mitochondrial membrane (O) as well as in the combined inner mitochondrial membrane (IMM) and matrix fraction (I) in ΔTom22 cells. Following N124K and K141D Tom22 expression, 3βHSD2 expression was restored in the IMM fraction, and Tom22 expression was restored in the OMM (O) fraction. (Bottom) VDAC2 expression was equally present in the OMM fraction irrespective of Tom22 knockdown. (G) Western blot analysis showing the expression of mitochondrial matrix-resident aldosterone synthase (AS) and P450scc (SCC) after incubating with different concentrations of Tom22 siRNA. (H) Western blot analysis showing the change in expression of 3βHSD2 after incubating two different concentrations of Tom22 siRNA with the MA-10 cells. (I) Metabolic conversion assays with MA-10 cells incubated with various concentrations of Tom22 siRNA, NAD, and [^{3}H]pregnenolone. The accumulated progesterone was identified by thin-layer chromatography. (Right) Quantitative measurement of the progesterone synthesized in the left panel. (J) Specificity of the 3βHSD2 antibody. Western blot analysis of the indicated amount of 3βHSD1 (AbCam) and 3βHSD2 (our homemade antibody) using antibodies specific for each. Our antibody recognizes only 3βHSD2; however, the commercially available 3βHSD1 antibody recognizes both 3βHSD2 and 3βHSD1. Data presented in panels D and I (right panel) represent the means plus SEM for three independent experiments performed at three different times.

the OMM and that 3βHSD2 is mostly at the OMM or near the OMM, indicating that these proteins are present at similar locations (Fig. 4F to H). Thus, the colocalization experiment suggests that 3βHSD2 (smaller 15-nm gold particle) is closely localized with Tom22 (55-nm gold particle). The cells not labeled with antibody are shown for a control (Fig. 4E). For another control, we performed the same colocalization experiment with nonsteroidogenic COS-1 cells, which express Tom22 but not 3βHSD2. As expected, 3βHSD2 was absent (Fig. 4I and J), although Tom22 was detected at the OMM (Fig. 4K and L). In summary, these results confirm that 3βHSD2 is present at the IMM and that Tom22 is present at the OMM.

Tom22 interacts directly with 3βHSD2. To determine whether Tom22 directly interacts with 3βHSD2, we performed coimmunoprecipitation analysis with antibodies specific for 3βHSD2, Tom22, VDAC2, and COX IV followed by immunoblotting with Tom22 and 3βHSD2 antibodies independently. As shown in Fig. 5A and B, a strong interaction between 3βHSD2 and Tom22 was detected in LM-permeabilized adrenals or gonadal tissues. Analysis of COX IV and VDAC2 (Fig. 5A and B) levels confirmed the presence of an equivalent amount of protein in each lane.

To understand how Tom22 may interact with other mitochondrial proteins, we performed chemical cross-linking using increasing concentrations of the chemical cross-linker BS^3 with mitochondria isolated from MA-10 cells. After blotting with both Tom22 and 3βHSD2 antibodies independently, a cross-linked protein band of approximately 60 kDa was identified with 0.03 mM BS^3 (Fig. 5C, arrowhead). Mass spectrometric analysis of this particular band identified both Tom22 (KLQMEQQQQLQQA, LQ MEQQQQL, and GATFDLSL) and 3βHSD2 (TVEWVGSLVDR, DPQLVPILIDAAR, and TSEWIGTLVEQHR) proteins. We also

TABLE 1 Identification of proteins within the LM-solubilized complex isolated by native gradient PAGE (3 to 16%) in MA-10 cells by mass spectrometry

GI no.[a]	Protein[b]	Peptide sequence[c]
840819	NADP transhydrogenase	K.TVAELEAEK.A
		K.AQYPIADLVK.M
6680932	Chromogranin A precursor	P.EPMQESKAEGNNQA.T
543890986	Cytochrome *b*-c_1 complex subunit 2	R.IIENLHDVAYK.N
6753036	Aldehyde dehydrogenase	K.LGPALATGNVVVMK.V + oxdn M
3851614	Succinate dehydrogenase	R.ILGSK.I
191500	Steroid 21 hydroxylase A	R.IPTFGCGAR.V
		K.TIEEALTQK.W
		R.LGLQDFVVVLNSNK.T
269914148	Cytochrome P450	K.LSGKMPPG.P
407341	Mitochondrial stress 70 protein	R.FEELNADLFR.S
		R.IINEPTAAAIAYGLDR.K
10716801	Tom22	K.LQMEQQQQLQQR.Q + oxdn M
6680748	ATP synthase subunit alpha	R.ILGADTSVDLEETGR.V
5762309	Microsomal glutathione *S*-transferase	F.LFFLAVGGV.Y
19526818	Phosphate carrier protein	R.YFPTQALNFAFK.D
13385726	Cytochrome *b*-c_1 complex subunit 7	R.GNNTTSLLSQSVAK.G
14269427	Triacylglycerol hydrolase	P.SSPPVVNT.V
148747566	Cholesterol side chain cleavage enzyme	K.TLVQVASYAMGR.E + oxdn M
		K.NFVPLLEGVAQDFIK.V
3851610	Succinate dehydrogenase Ip subunit	R.LGANSLLDLVVFGR.A
6680027	Glutamate dehydrogenase 1	K.IIAEGANGPTTPEADK.I
9653733	Aldosterone synthase	V.FRELGPIF.R
		P.KSLTRWTS.T
2613145	3β-Hydroxysteroid dehydrogenase 2	K.TVEWVGSLVDR.H
		R.QTILTVNLK.G
		K.TSEWIGTLVEQHR.E
6680618	Medium-chain specific acyl-CoA dehydrogenase	P.DPKVPASK.A

[a] GI no., GeneInfo identifier number.
[b] CoA, coenzyme A.
[c] Periods after the first letters of sequences indicate the N-terminal side, and periods before the last letters indicate the C-terminal side. oxdn M, oxidized M.

TABLE 2 Identification of proteins within the LM-solubilized complex isolated by 2D native gradient PAGE (3 to 16%) in MA-10 cells by mass spectrometry

GI no.[a]	Protein	Peptide sequence[b]
464506	Pyruvate carboxylase	R.VFDYSEYWEGAR.G
6680932	Chromogranin A precursor	P.EPMQESKAEGNNQA.T
3851614	Succinate dehydrogenase Fp subunit	R.ILGSK.I
		R.LGANSLLDLVVFGR.A
191500	Steroid 21 hydroxylase A	R.IPTFGCGAR.V
		K.TIEEALTQK.W
		R.LGLQDFVVVLNSNK.T
6753036	Aldehyde dehydrogenase	R.TEQGPQVDETQFK.K
		R.AFPAWADTSILSR.Q
19526818	Phosphate carrier protein	R.YFPTQALNFAFK.D
149029483	ATP synthase	R.ILGADTSVDLEETGR.V
11177910	HSP70	K.CNEVIR.W
		K.VEIIANDQGNR.T
		R.DLGYVPLVSWEEAK.Q
238336	3β-Hydroxysteroid dehydrogenase	K.LTVLEGDILDEPFLK.R
10716801	Tom22	K.LQMEQQQQLQQR.Q + oxdn M
2257955	Cytochrome b_5	K.TYIIGELHPDDR.S
13385726	Cytochrome *b*-c_1 complex	R.IQEVDAQMLR.D + oxdn M
6680748	ATP synthase subunit alpha	R.ILGADTSVDLEETGR.V
34538601	Cytochrome *c* oxidase subunit II	R.VVLPMELPIR.M + oxdn M

[a] GI no., GeneInfo identifier number.
[b] Periods after the first letters of sequences indicate the N-terminal side, and periods before the last letters indicate the C-terminal side. oxdn M, oxidized M.

cross-linked MA-10 cells *in vivo* with various concentrations of BS^3 to examine the interaction between 3βHSD2 and Tom22 in a similar fashion as performed previously (49). Interaction between 3βHSD2 and Tom22 was initiated with 2 mM BS^3, and band intensity increased with increasing cross-linker concentrations, decreasing with ≥5 mM cross-linker (Fig. 5D). The 60-kDa band was due to the newly generated cross-linked product, confirming that the Tom22 protein interacted with 3βHSD2 (Fig. 5D). Identical results were observed when probed with the Tom22 antibody. However, the 60-kDa band was absent after probing with antibodies specific for VDAC2 and Tom40 (Fig. 5D). Thus, 3βHSD2 and Tom22 interact each other in the mitochondria, possibly through the C terminus of Tom22 exposed to the IMS (47).

To determine how closely these two proteins interact, we performed density gradient centrifugation for 2 and 4 h followed by Western blotting with Tom22 and 3βHSD2 antibodies. In the presence of LM, fractions 8 to 11 overlapped at 2 h (Fig. 5E). The density gradients in the bottom panels were digitized to generate the top panels (Fig. 5E and F). At 4 h, Tom22 showed a good distribution profile (Fig. 5F); however, the distribution of 3βHSD2 moved to fractions 10 to 14 (Fig. 5F). These results suggest that the interaction between Tom22 and 3βHSD2 is strong but transient and not mediated by covalent linkages or embedded in each other through the vesicles. The density distribution of the outer mitochondrial resident VDAC2 or Tom40 was identical to the distribution pattern that we observed earlier (49).

Identification of the amino acids mediating Tom22-3βHSD2 interaction. As 3βHSD2 is active only at the IMS, its interaction with Tom22 is most likely through the unstructured amino acids spanning positions 128 to 142 of Tom22. Although a smaller transmembrane loop with basic amino acids may participate in the interaction, its short length makes this less likely. Since Tom22 has many unstructured regions (50), it remains very flexible while associated with the membrane. The partially developed three-dimensional solution structure predicted that Tom22 should have a

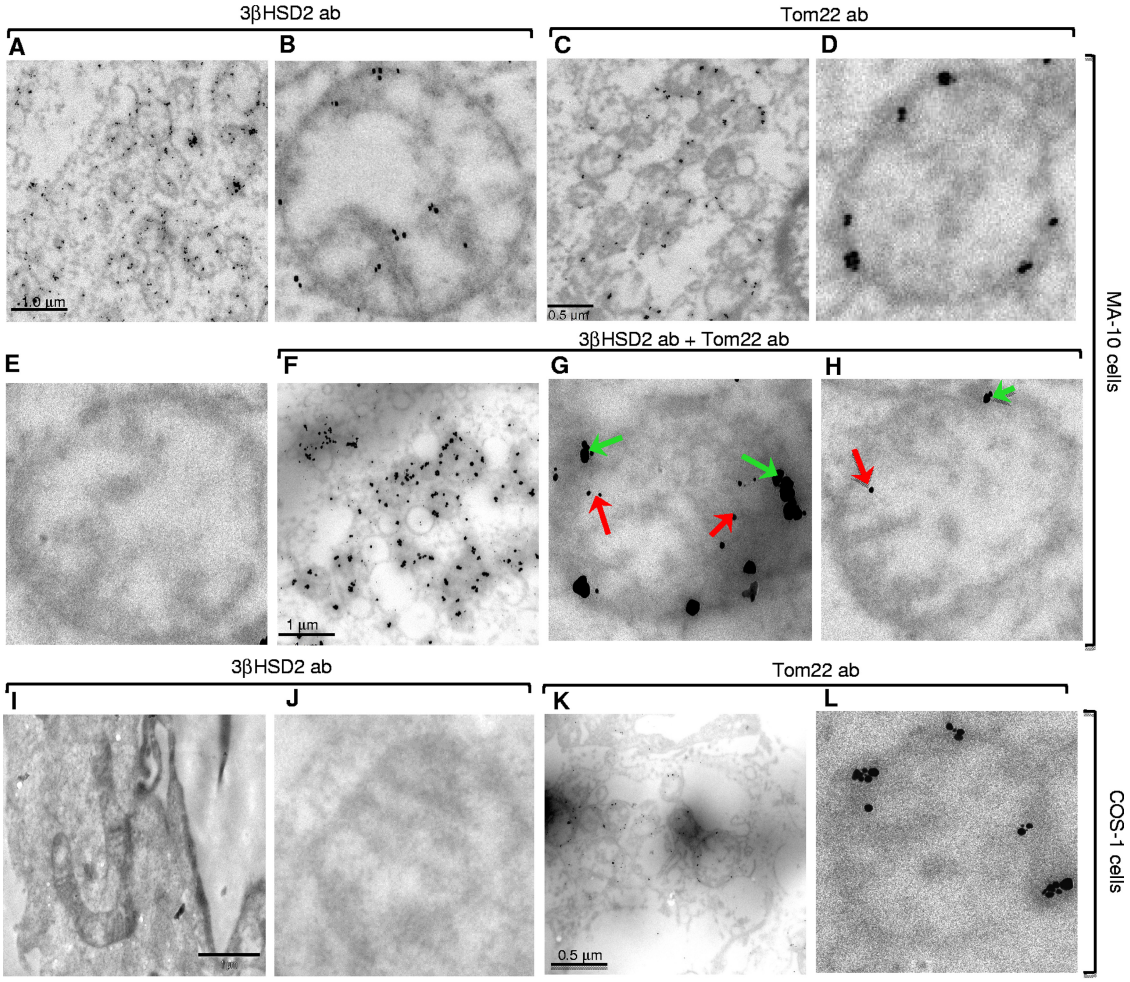

FIG 4 Localization of 3βHSD2 and Tom22 by immune electron microscopy (EM). (A to H) Localization of 3βHSD2 (A and B) or Tom22 (C and D) in a MA-10 cell where most of the 3βHSD2 was localized to the cristae and OMM (B), and Tom22 is localized at the OMM (D). Panels B and D show a higher magnification of a mitochondrion. (E) Visualization of the mitochondrial structure in the absence of any antibody. (F to H) Visualization of the mitochondrion with Tom22 and 3βHSD2 antibodies together in a MA-10 cell. For 3βHSD2, the gold particle was 15 nm (red arrows), whereas the particle size was 55 nm for Tom22 (green arrows). Panels G and H show a higher magnification of a mitochondrion after double labeling. (I to L) COS-1 cells were incubated with antibodies specific for 3βHSD2 (I and J), confirming its absence, and Tom22 expression in mitochondria (K and L). Panel K is a higher-magnification image of a COS-1 cell mitochondrion labeled with Tom22 and 3βHSD2 antibodies. Bars, 1.0 μm (A and F), 0.5 μm (C and K), and is 2.0 μm (I).

minimum amino acid region facing the IMS, comprising amino acids 128 to 142 (50). To confirm that the C terminus of Tom22 is indeed responsible for its interaction with 3βHSD2, we expressed various Tom22 mutants, N124K, S128G, S137G, and K141D, in MA-10 cells expressing Tom22 siRNA (Fig. 6A). Western blot analysis confirmed overexpression of WT or mutant Tom22 expression in these cells (Fig. 6A). Also, expression of 3βHSD2 and VDAC2 was very similar (Fig. 6A). Since Tom22 expression is associated with 3βHSD2, we next examined pregnenolone-to-progesterone conversion following expression of the C-terminal Tom22 mutants (25). Whereas WT MA-10 cells synthesized 97 ng/ml of progesterone, the N124K mutant synthesized 61 ng/ml, which is about 60% (Fig. 6B and C). All of the other mutants synthesized progesterone levels in the range of 20 to 25 ng/ml, suggesting that these amino acids are responsible for Tom22 interaction with 3βHSD2 (Fig. 6B and C). According to the partial nuclear magnetic resonance (NMR) structure (50), all mutations in the unstructured region of the Tom22 reduced progesterone synthesis (Fig. 6B and C), possibly through its inability to interact with 3βHSD2. Furthermore, the S128G mutation, which is present in the α-helical region, likely altered the conformation, reducing 3βHSD2 activity (Fig. 6B and C). The N124K mutation within the membrane-spanning region did not alter progesterone levels, suggesting that only IMS-exposed amino acids participate in the interaction with 3βHSD2. Indeed, coimmunoprecipitation (co-IP) analysis showed that only WT and N124K Tom22 interacted with 3βHSD2 (Fig. 6D). In addition, immunoelectron microscopy confirmed that both 3βHSD2 and Tom22 were almost completely absent at the mitochondria in ΔTom22 MA-10 cells (Fig. 6G). However, expression of the Tom22 mutants restored its levels along with 3βHSD2 expression to levels similar to that observed in the WT cells (Fig. 6H and I versus F).

To understand the impact of the absence of Tom22 on 3βHSD2 mRNA expression, we isolated mRNA from the

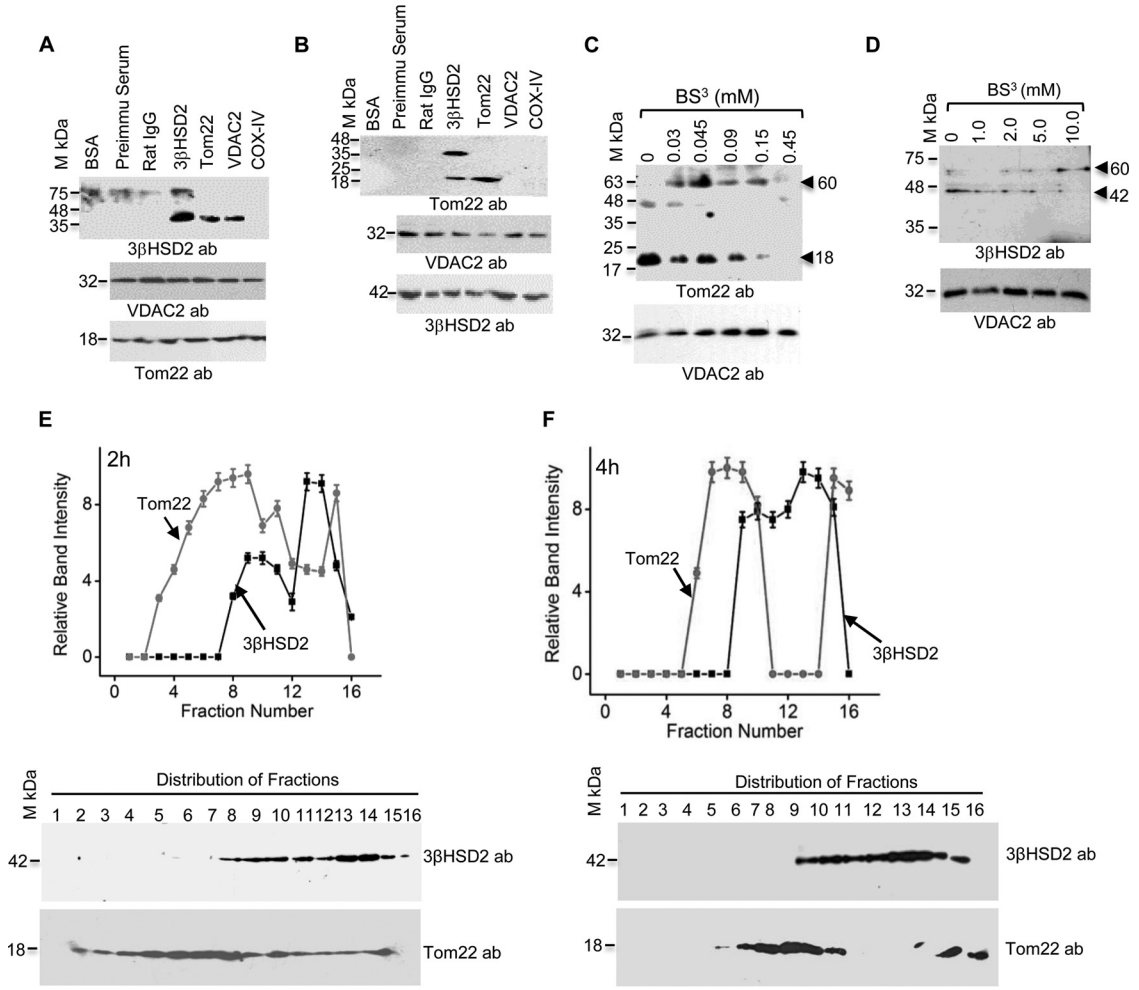

FIG 5 3βHSD2 directly interacts with Tom22. (A and B) Coimmunoprecipitation of MA-10 cells incubated with 0.3% LM overnight and then immunoprecipitated with the indicated antibodies followed by Western blotting with 3βHSD2 and Tom22 antibodies. The cross-linked products were separated by 12% SDS-PAGE (A) and 16% SDS-PAGE (B). The bottom panels show Western blotting with VDAC2 and Tom22 or 3βHSD2 antibodies prior to cross-linking. Preimmu, preimmune. (C) *In vitro* chemical cross-linking of the mitochondria isolated from mouse adrenals permeabilized with LM, cross-linked with various concentrations of BS^3, and then separated by 12% SDS-PAGE, followed by Western blotting with Tom22 antibody. A new 60-kDa protein was apparent due to Tom22 and 3βHSD2 interaction. (D) After chemical cross-linking of MA-10 cells with BS^3, the cells were lysed with LM, and identification of the chemical cross-linked protein bands was performed by electrophoresis on 16% SDS-polyacrylamide gels followed by Western blotting with 3βHSD2 antibody. The bottom gels in panels C and D show the protein levels prior to cross-linking stained with VDAC2 antibody, confirming that an identical amount of protein was employed in each experiment. (E and F) Localization of the proteins associated with Tom22 and 3βHSD2 through sucrose density gradient after 2 h and 4 h of ultracentrifugation. Each fraction was probed with the indicated antibodies, and the distribution of the proteins was graphed. Data presented are the means ± SEM for three independent experiments. The bottom panels show representative density gradient fractionation and Western blotting with the indicated antibodies.

ΔTom22 and WT MA-10 cells and performed RT-PCR analysis. As shown in Fig. 6J, 3βHSD2 mRNA was greatly reduced following Tom22 silencing. Because Tom22 knockdown did not affect the expression of StAR or inner mitochondrial proteins associated with the TIM23 complex (25), the effect of Tom22 knockdown is specific to 3βHSD2.

We next sought to determine the portion of 3βHSD2 that interacts with Tom22, hypothesizing that it is mediated by its C terminus following mitochondrial import. 3βHSD2 mutants with 3, 10, 20, and 30 amino acids deleted from the C terminus were expressed in COS-1 cells in the presence of the F2 vector. As shown in Fig. 7A, 3βHSD2 activity was reduced with the deletion of 3 and 10 amino acids from the C terminus compared to WT 3βHSD2 (the total amount of steroid per milliliter was generated from 20 mg of mitochondrial protein and was 570 ng and 180 ng versus 830 ng, respectively). The activity was further reduced with deletion of 20 amino acids to a level similar to that of the buffer control (~57 ng) (Fig. 7A, bottom panel). A more detailed analysis of the first 10 C-terminal amino acids of 3βHSD2 revealed that although progesterone conversion was retained, it was almost 50% less than that derived from WT 3βHSD2 (Fig. 7B). Upon deletion of the 7th amino acid, the activity was reduced by 75%, and activity was completely ablated with deletion of 8 to 10 C-terminal amino acids (Fig. 7B). Western blot analysis of the deletion mutants confirmed similar levels of expression for all of the C-terminus-deleted constructs (Fig. 7C).

To confirm that the interaction of Tom22 is indeed compromised by deleting the C-terminal amino acids of 3βHSD2, coim-

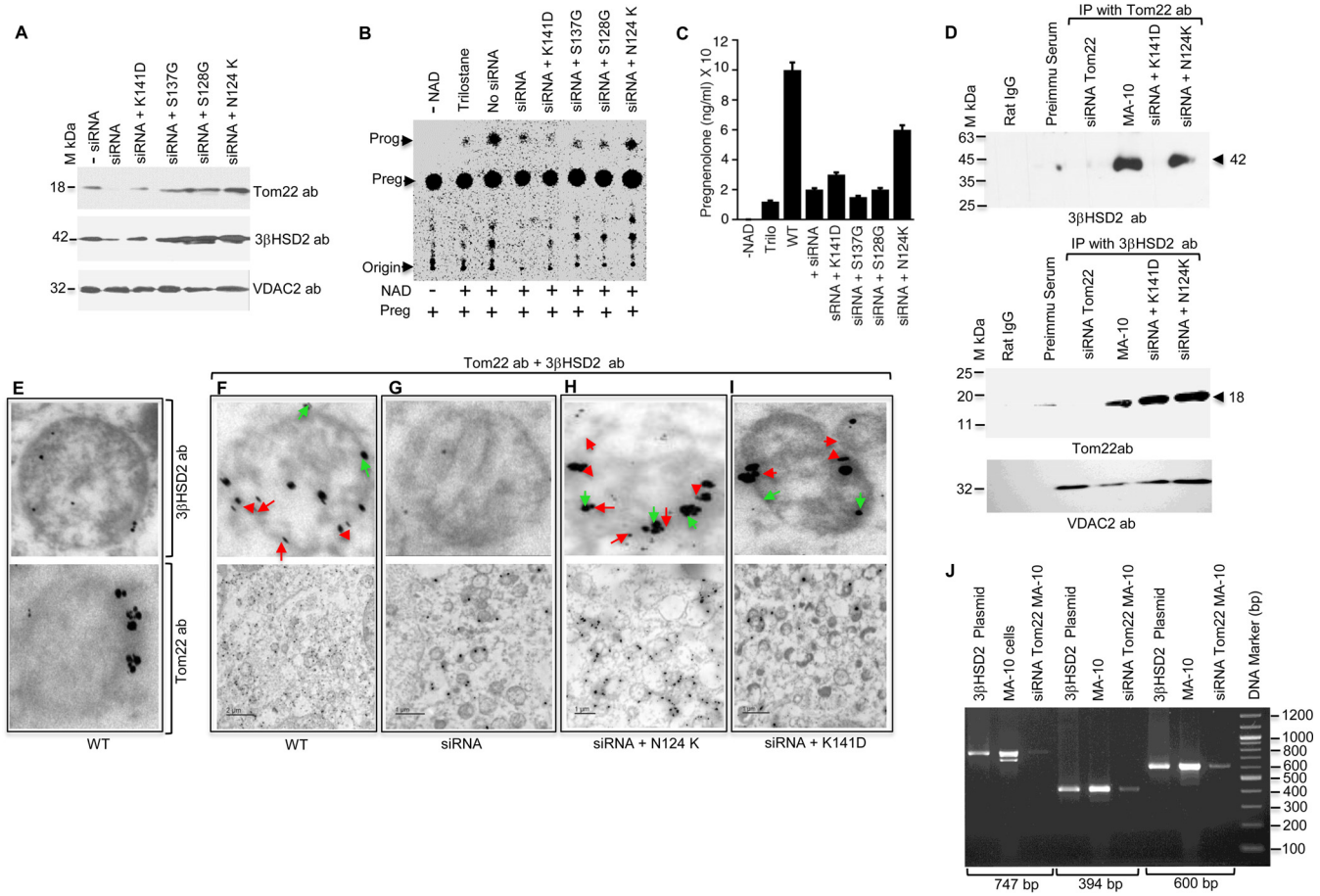

FIG 6 Role of the C terminus of Tom22 in regulating 3βHSD2 metabolic activity. (A) The indicated Tom22 point mutants were expressed in MA-10 cells after knocking down Tom22 with 60 pmol of siRNA. Western blot analysis was performed using Tom22, 3βHSD2, and VDAC2 antibodies, confirming the equal expression of each. Expression remained unchanged with negative (−) siRNA. (B) Pregnenolone-to-progesterone conversion by ΔTom22 MA-10 cells overexpressing the indicated mutants. (C) Quantitative measurement of the progesterone synthesized. Data represent the means plus SEM for three independent experiments performed at three different times. (D) Co-IP analysis with 3βHSD2 antibodies after Tom22 knockdown and expression of the indicated mutants in MA-10 cells. The blots were stained with 3βHSD2 and Tom22 antibodies independently. The bottom panel shows VDAC2 expression, showing the same amount of cells were used for each experiment. (E to I) Electron microscopy of Tom22 mutants (F to I) in ΔTom22 MA-10 cells. (E) Typical pattern of an enlarged view of mitochondrion stained with 3βHSD2 and Tom22 antibodies. (F) Expression pattern of Tom22 (bottom panel), and the top panel shows its typical localization in a mitochondrion. The small gold particles (15 nm, red arrowheads) are 3βHSD2, and the larger 55-nm particles are Tom22 (green arrows). (G) Tom22 expression is absent in ΔTom22 MA-10 cells, and the top panel shows only one mitochondrion with minimal Tom22. (F and G) Expression of Tom22 in wild-type (F) and siRNA knockdown (G) MA-10 cells. (H and I) Bottom panels show expression of N124K (H) and K141D (I) Tom22 in ΔTom22 MA-10 cells. The top panels show an enlarged mitochondrion from the bottom panel. Bars, 2.0 μm (F) and 1.0 μm (G to I). (J) RT-PCR amplification of cDNA from ΔTom22 MA-10 cells with different 3βHSD2-nested primers showing amplification of 747-bp, 394-bp, and 600-bp cDNA. The human 3βHSD2 plasmid DNA was the control for the PCR, and WT MA-10 cDNA was used as internal control for the siRNA knockdown. The positions of DNA markers (in base pairs) are shown to the right of the gel.

munoprecipitation analysis was undertaken. As shown in Fig. 7D, immunoprecipitation with a Tom22 antibody followed by Western blotting with 3βHSD2-specific antibody revealed that deletion of more than seven C-terminal amino acids from 3βHSD2 reduced its interaction with Tom22. However, the expression of Tom22 or VDAC2 remained unchanged. Western blot analysis confirmed that the 3βHSD2 C-terminal deletion mutants were present at the IMM (I lanes) after overexpression in COS-1 cells (Fig. 7E). Probing the same membrane with a VDAC2 antibody showed its presence at the OMM (Fig. 7E, O lanes), confirming the accuracy of the organelle fractionation. Thus, our results strongly confirm that the C terminus of 3βHSD2 is necessary for its interaction with Tom22. Colocalization analysis of WT and mutant 3βHSD2 with Tom22 using immunoelectron microscopy (Fig. 8) revealed that the expression level of each C-terminal truncated mutant was similar, suggesting a possible change in 3βHSD2 conformation that inhibits its interaction with Tom22 at the IMS.

DISCUSSION

The mitochondrial import channel, TOM40, consists of several high- and low-molecular-weight Tom proteins facing primarily the cytoplasmic side of the OMM. Tom22, present at the OMM, is the crucial import receptor, spanning from the outer membrane by its central transmembrane segment, with most of its N-terminal amino acids and a short segment of C-terminal amino acids exposed to the cytosol and IMS, respectively (18, 51). The cytosolic domains of Tom20 and Tom22 cooperate to form a prese-

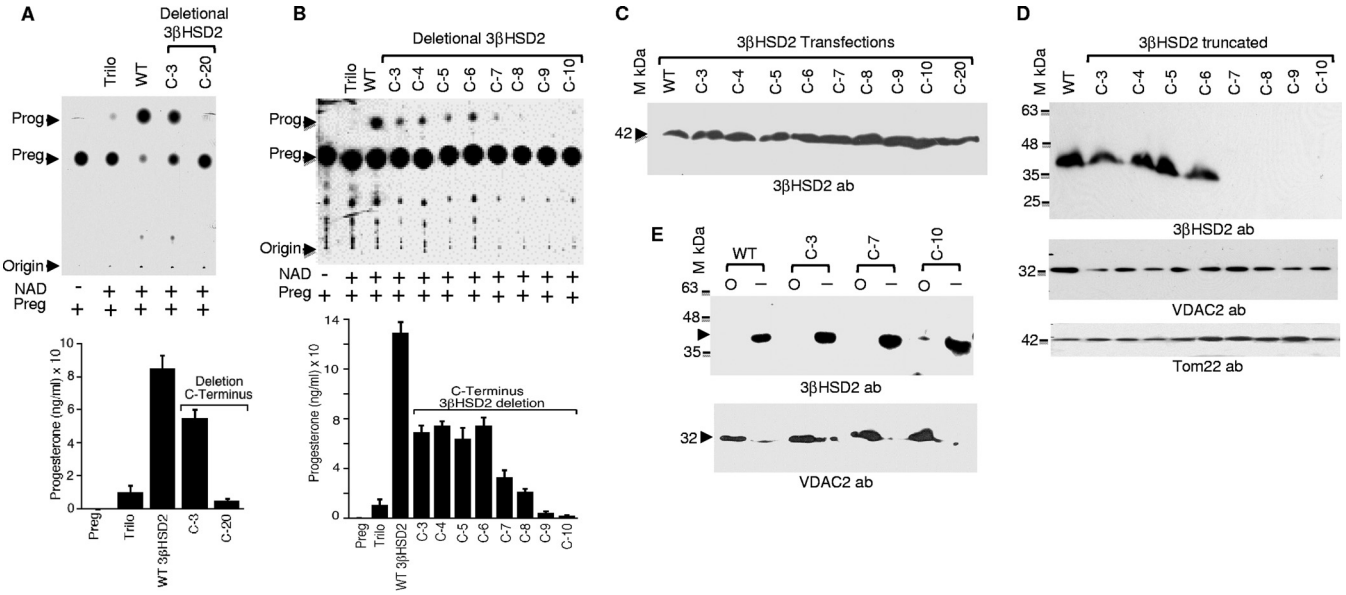

FIG 7 The C terminus of 3βHSD2 is required for interaction with Tom22. (A and B) Metabolic activity of COS-1 cells transfected with the indicated deletion mutants and F2. (Bottom) Quantitative measurement of the amount of progesterone synthesized after three independent transfections performed at three different times. (C) Western blot analysis of COS-1 cells transfected with the indicated C-terminal deletion mutants of 3βHSD2. (D) Coimmunoprecipitation of the lysates isolated from panel C with Tom22 antibodies followed by blotting with 3βHSD2 antibodies. (Bottom) Tom22 and VDAC2 antibodies were employed to provide the evidence of identical loading. (E) Outer (O) and inner (I) mitochondrial fractionation and localization of the WT, C-3, C-7, and C-10 3βHSD2 after overexpression in COS-1 cells and staining with a 3βHSD2 antibody. The bottom panel was stained with a VDAC2 antibody, confirming that an equivalent amount of total protein was present in each lane.

quence receptor to recognize mitochondrial targeting signals (19, 52–54). Tom22 interacts with the polar surface of the amphipathic presequences through its negatively charged acid-rich region (15, 16, 18, 23). However, Tom22 does not participate in the mitochondrial translocation of steroidogenic proteins, including cytochrome P450scc, AS, and StAR (49). These results suggest that proteins can reach the mitochondria without the direct assistance of Tom22. Because the dynamic interactions between the IMS domain of Tom22 and Tim50 promote transfer of mitochondrial presequences from Tom22 to Tim50, this transient interaction may bring the TIM23 complex closer to the TOM40 complex. As a result, the interaction and processing of incoming presequences are facilitated efficiently through the TIM23 complex (55), which may account for 3βHSD2 association with the Tim50-Tim23 complex in steroidogenic cells from adrenals and gonads (25).

The single- and double-labeling EM experiments with MA-10 cells showed that 3βHSD2 is principally at the IMS, where it is active and requires the mitochondrial proton gradient to initiate the metabolic reaction, with a smaller fraction at the OMM, whereas Tom22 remains at the OMM. However, the interaction between 3βHSD2 and Tom22 was confirmed with coimmunoprecipitation, density gradient separation, and cross-linking studies. Thus, immediately after mitochondrial translocation, 3βHSD2 may require a membrane to open its conformation partially (43).

During the acute regulation of steroidogenesis, the abnormally higher expression of steroidogenic proteins may compete for mitochondrial entry (32), possibly displacing Tom22. Also, a large flow of cholesterol transport is necessary, possibly through the electrolyte import channel, although this has not been fully elucidated. Thus, the Tom22-specific interaction site numbers become smaller than expected. The high concentration of binding sites for presequence peptides most likely shortens the transient time necessary for import. The interaction of 3βHSD2 with Tom22 is facilitated by the presence of Tim50 (25), which associates with 3βHSD2 in a loose manner possibly in its partially open conformation (56). As a result, Tim23 forces the N-terminal region of 3βHSD2 to interact with Tom22. The interaction between Tom22 and 3βHSD2 is possibly enhanced by 3βHSD2 entry mediated by the region from amino acids 283 to 310, as the absence of this region prevents its mitochondrial import. A model describing gradual translocation of 3βHSD2 into the mitochondria and its association with the IMS-exposed C terminus of Tom22 is presented in Fig. 9. 3βHSD2 possesses the catalytic activity for a transient, stable conformation required for interaction with the C terminus of Tom22, which faces the IMS, resulting in a free N-terminal region of 3βHSD2. Thus, 3βHSD2 remains in a transiently pseudostable conformation, minimizing the energetic cost, which may account for its isomerase and dehydrogenase activities in which the same substrate is used with various minimum energetic stabilization at the same time. However, the conversion of these metabolic activities does not happen one after the other, but after the synthesis of several other metabolic activities. Thus, the conformation change is necessary, as both states must be separated with a minimum difference in stability (56), and this change will require interaction with a close protein, such as Tom22.

How this open state is possible at the IMS remains to be determined. We hypothesize that 3βHSD2 connects the IMM with the OMM, interacting with Tom22 via its free amino acids, but not through the membrane-associated amino acids, as changing amino acid 124 from serine to glycine did not alter metabolic activity. Mass spectrometric analysis also identified cofactor en-

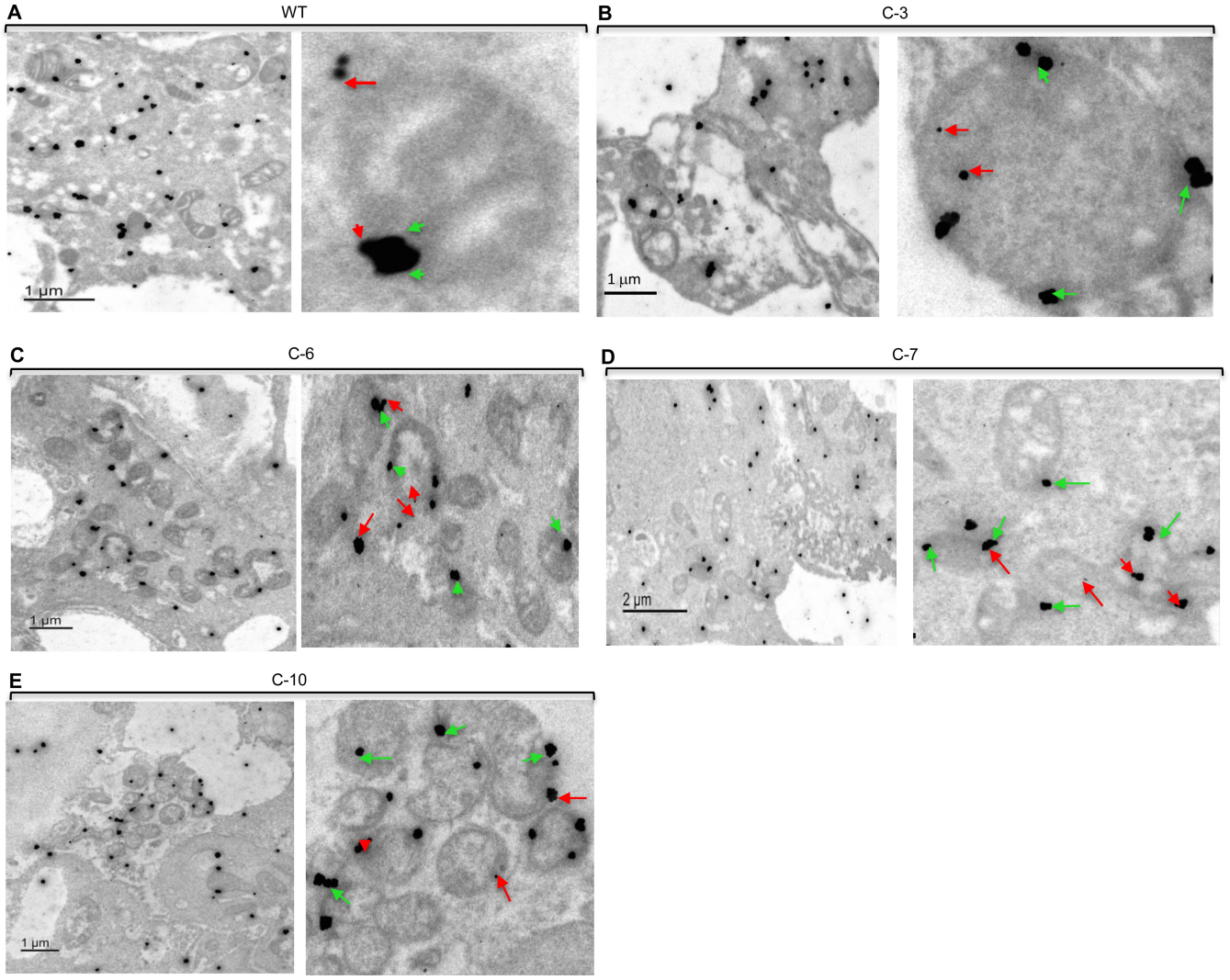

FIG 8 Localization of WT 3βHSD2, C-terminal deletion mutants of 3βHSD2 and Tom22 by immune electron microscopy (EM). EM was undertaken by double labeling with independent antibodies together after overexpression of WT 3βHSD2 and its C-terminal deletion mutants in COS-1 cells. (A) Colocalization of 3βHSD2 and Tom22. (B to E) Localization of C-terminal truncated 3βHSD2 and Tom22. The right panels show an enlarged view of a mitochondrion or a few mitochondria closely associated from the respective left panel. The small 15-nm gold particles (red arrows) show 3βHSD2, and the big 55-nm gold particles indicate Tom22 (green arrows). For 3βHSD2, the gold particle was 15 nm (red arrow); the particle size was 55 nm for Tom22 (green arrow).

zymes in the 500-kDa complex, suggesting that 3βHSD2, Tom22, and cofactors all work at the same time. Our unpublished observation with cyclic AMP (cAMP) stimulation showed almost no enhanced expression of 3βHSD2; however, its metabolic activity was increased. Therefore, it is likely that there is an increase in 3βHSD2 import from the outer to the IMS to enhance metabolic capacity. However, in the absence of Tom22, the 3βHSD2 complex was incomplete, resulting in reduced metabolic activity. In case the IMS-exposed sequence is longer, the interaction with 3βHSD2 may be mediated through an exposed helical form of Tom22 and is expected to be a permanent interaction. Thus, a transient interaction may be necessary for 3βHSD2 to have more than one activity. The presence of a small segment of Tom22 allows for flexible interaction with 3βHSD2 as an off-and-on mechanism for isomerase and dehydrogenase activities. In the case of mutant Tom22, the triangular interaction between Tom22-NAD-3βHSD2 should occur at the same time. In the absence of Tom22 or in the event of a Tom22 mutation, the orientation of 3βHSD2 would not be the same as observed for the WT protein, resulting in reduced or absent progesterone synthesis. The report describing a patient with ambiguous genitalia and borderline reduced steroids but no 3βHSD2 mutation (8) may now be explained by the role of Tom22 in steroid synthesis.

Our mechanism reported here also explains why patients with congenital adrenal hyperplasia due to mutation in the 3βHSD2 protein still have 10 to 15% progesterone synthesis. Because the mutants are conformationally different from the WT protein, they may bind the substrate, NADH, and Tom22 in a different fashion, resulting in a minimal level of activity (8). The reduced catalytic activity will be dependent upon the degree to which the mutation affects the protein conformation. Thus, Tom22 is physiologically required to form a complex with 3βHSD2, resulting in an appropriate conformation to initiate metabolic activity with NAD. In

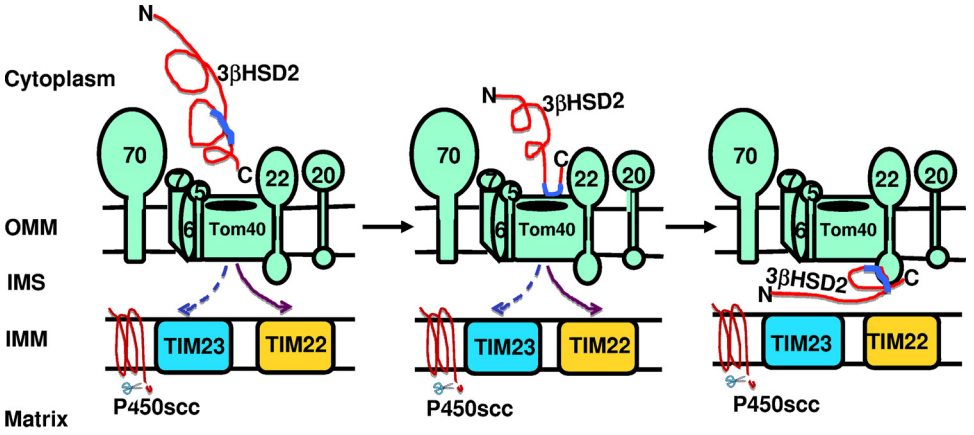

FIG 9 Schematic presentation of 3βHSD2 translocation through the mitochondrial Tom40 import channel and association with the IMS-exposed Tom22. In the first step, newly synthesized 3βHSD2 is processed for mitochondrial import through the Tom40 import channel. The translocases are indicated in their appropriate position. In the second step, 3βHSD2 moves closer to the mitochondrial import pore and is imported through the region from amino acids 283 to 310 as a signal sequence (blue). In the final step, following import into the IMS, the 283-310 amino acid region is associated with the IMS-exposed region of Tom22 for participating in metabolic activity. IMM, inner mitochondrial membrane; IMS, intermembrane space; OMM, outer mitochondrial membrane.

summary, we conclude that 3βHSD2 requires an interaction with Tom22 for pregnenolone-to-progesterone conversion in steroidogenic cells.

ACKNOWLEDGMENTS

This work was supported by a grant from the National Institutes of Health (057876) and a grant from the Anderson Cancer Institute to H.S.B.

FUNDING INFORMATION

HHS | NIH | National Institute of Child Health and Human Development (NICHD) provided funding to Himangshu S Bose under grant number 057876.

REFERENCES

1. **Acland P, Dixon M, Peters G, Dickson C.** 1990. Subcellular fate of the Int-2 oncoprotein is determined by choice of initiation codon. Nature **343:**662–665. http://dx.doi.org/10.1038/343662a0.
2. **Glick BS, Brandt A, Cunningham K, Muller S, Hallberg RL, Schatz G.** 1992. Cytochrome c1 and b2 are sorted to the intermembrane space of yeast mitochondria by a stop-transfer mechanism. Cell **69:**347–357.
3. **Simard J, Ricketts M-L, Gingras S, Soucy P, Feltus FA, Melner MH.** 2005. Molecular biology of the 3β-hydroxysteroid dehydrogenase/Δ5-Δ4 isomerase gene family. Endocr Rev **26:**525–582. http://dx.doi.org/10.1210/er.2002-0050.
4. **Miller WL, Auchus RJ.** 2011. The molecular biology, biochemistry, and physiology of human steroidogenesis and its disorders. Endocr Rev **32:**81–151. http://dx.doi.org/10.1210/er.2010-0013.
5. **Labrie F, Luu-The V, Labrie C, Simard J.** 2001. DHEA and its transformation into androgens and estrogens in peripheral target tissues: intracrinology. Front Neuroendocrinol **22:**185–212. http://dx.doi.org/10.1006/frne.2001.0216.
6. **Nair KS, Rizza RA, O'Brien P, Dhatariya K, Short KP, Nehra A, Vittone JL, Klee GG, Basu A, Basu R, Cobelli C, Toffolo G, Man CD, Tindall DJ, Melton LJ, Smith GE, Khosla S, Jensen MD.** 2006. DHEA in elderly women and DHEA or testosterone in elderly men. N Engl J Med **355:**1647–1659. http://dx.doi.org/10.1056/NEJMoa054629.
7. **Welzel M, Wustemann N, Simic-Schleicher G, Dorr HG, Schulze E, Shaikh G, Clayton P, Grotzinger J, Holterhus P-M, Riepe FG.** 2008. Carboxy-terminal mutations in 3β-hydroxysteroid dehydrogenase type II cause severe salt-wasting congenital adrenal hyperplasia. J Clin Endocrinol Metab **93:**1418–1425. http://dx.doi.org/10.1210/jc.2007-1874.
8. **Morel Y, Roucher F, Plotton I, Simard J, Coll M.** 2014. 3β-Hydroxysteroid dehydrogenase deficiency, p 99–110. *In* New MI, Lekarev O, Parsa A, Yuen T, O'Malley B, Hammer G (ed), Genetic steroid disorders. Elsevier Inc., Waltham, MA.
9. **Mayer A, Neupert W, Lill R.** 1995. Mitochondrial protein import: reversible binding of the presequence at the trans side of the outer membrane drives partial translocation and unfolding. Cell **80:**127–137. http://dx.doi.org/10.1016/0092-8674(95)90457-3.
10. **Rapaport D, Neupert W, Lill R.** 1997. Mitochondrial protein import. Tom40 plays a major role in targeting and translocation of preproteins by forming a specific binding site for the presequence. J Biol Chem **272:**18725–18731.
11. **Moczko M, Bomer U, Kubrich M, Zufall N, Honlinger A, Pfanner N.** 1997. The intermembrane space domain of mitochondrial Tom22 functions as a trans binding site for preproteins with N-terminal targeting sequences. Mol Cell Biol **17:**6574–6584. http://dx.doi.org/10.1128/MCB.17.11.6574.
12. **Kanamori T, Nishikawa S, Nakai M, Shin I, Schultz PG, Endo T.** 1999. Uncoupling of transfer of the presequence and unfolding of the mature domain in precursor translocation across the mitochondrial outer membrane. Proc Natl Acad Sci U S A **96:**3634–3639. http://dx.doi.org/10.1073/pnas.96.7.3634.
13. **Esaki M, Shimizu H, Ono T, Yamamoto H, Kanamori T, Nishikawa S, Endo T.** 2004. Mitochondrial protein import. Requirement of presequence elements and tom components for precursor binding to the TOM complex. J Biol Chem **279:**45701–45707.
14. **Qiu J, Wenz L, Zerbes RM, Oeljeklaus S, Bohnert M, Stroud DA, Wirth C, Ellenrieder L, Thornton N, Kutik S, Wiese S, Schulze-Specking A, Zufall N, Chacinska A, Guiard B, Hunte C, Warscheid B, van der Laan M, Pfanner N, Wiedemann N, Becker T.** 2013. Coupling of mitochondrial import and export translocases by receptor-mediated supercomplex formation. Cell **154:**596–608. http://dx.doi.org/10.1016/j.cell.2013.06.033.
15. **Neupert W, Herrmann JM.** 2007. Translocation of proteins into mitochondria. Annu Rev Biochem **76:**723–729. http://dx.doi.org/10.1146/annurev.biochem.76.052705.163409.
16. **Chacinska A, Koehler CM, Milenkovic D, Lithgow T, Pfanner N.** 2009. Importing mitochondrial proteins: machineries and mechanisms. Cell **138:**628–644. http://dx.doi.org/10.1016/j.cell.2009.08.005.
17. **Bose HS, Lingappa VR, Miller WL.** 2002. The steroidogenic acute regulatory protein, StAR, works only at the outer mitochondrial membrane. Endocr Res **28:**295–308. http://dx.doi.org/10.1081/ERC-120016800.
18. **Lithgow T, Junne T, Suda T, Gratzer S, Schatz G.** 1994. The mitochondrial outer membrane protein MAS22p is essential for protein import and viability of yeast. Proc Natl Acad Sci U S A **91:**11973–11977. http://dx.doi.org/10.1073/pnas.91.25.11973.
19. **Bolliger L, Junne T, Schatz G, Lithgow T.** 1995. Acidic receptor domains on both sides of the outer membrane mediate translocation of precursor proteins into yeast mitochondria. EMBO J **14:**6318–6326.
20. **Dekker PJ, Ryan MT, Brix J, Muller H, Honlinger A, Pfanner N.** 1998. Preprotein translocase of the outer mitochondrial membrane: molecular

dissection and assembly of the general import pore complex. Mol Cell Biol **18:**6515–6524. http://dx.doi.org/10.1128/MCB.18.11.6515.
21. **van Wilpe S, Ryan MT, Hill K, Maarse AC, Meisinger C, Brix J, Dekker PJ, Mocsko M, Wagner R, Meijer M, Guiard B, Honlinger A, Pfanner N.** 1999. Tom22 is a multifunctional organizer of the mitochondrial preprotein translocase. Nature **401:**485–489. http://dx.doi.org/10.1038/46802.
22. **Mayer A, Nargang FE, Neupert W, Lill R.** 1995. MOM22 is a receptor for mitochondrial targeting sequences and cooperates with MOM19. EMBO J **14:**4204–4211.
23. **Hulett JM, Lueder F, Chan NC, Perry AJ, Wolynec P, Likić VA, Gooley PR, Lithgow T.** 2008. The transmembrane segment of Tom20 is recognized by Mim1 for docking to the mitochondrial TOM complex. J Mol Biol **376:**694–704. http://dx.doi.org/10.1016/j.jmb.2007.12.021.
24. **Bose HS, Lingappa VR, Miller WL.** 2002. Rapid regulation of steroidogenesis by mitochondrial protein import. Nature **417:**87–91. http://dx.doi.org/10.1038/417087a.
25. **Pawlak KJ, Prasad M, Thomas JL, Whittal RM, Bose HS.** 2011. Inner mitochondrial translocase Tim50 interacts with 3beta-hydroxysteroid dehydrogenase type-2 to regulate adrenal and gonadal steroidogenesis. J Biol Chem **286:**39130–39140. http://dx.doi.org/10.1074/jbc.M111.290031.
26. **Adams BP, Bose HS.** 2012. Alteration in accumulated aldosterone due to N-terminal cleavage of aldosterone synthase. Mol Pharm **81:**465–474. http://dx.doi.org/10.1124/mol.111.076471.
27. **Dettmer U, Newman AJ, Luth ES, Bartels ES, Selkoe D.** 2013. In vivo cross-linking reveals principally oligomeric forms of α-synuclein and β-synuclein in neurons and non-neuronal cells. J Biol Chem **288:**6371–6385. http://dx.doi.org/10.1074/jbc.M112.403311.
28. **Bose M, Debnath D, Chen Y, Bose HS.** 2007. Folding, activity and import of steroidogenic acute regulatory protein (StAR) into mitochondria changed by nicotine exposure. J Mol Endocrinol **39:**67–79. http://dx.doi.org/10.1677/JME-07-0051.
29. **Schwartz MP, Matouschek A.** 1999. The dimensions of the protein import channels in the outer and inner mitochondrial membrane. Proc Natl Acad Sci U S A **96:**13086–13090. http://dx.doi.org/10.1073/pnas.96.23.13086.
30. **Bose M, Adams BP, Whittal RM, Bose HS.** 2008. Identification of unknown protein complex members by radiolocalization and analysis of low-abundance complexes resolved using native PAGE. Electrophoresis **29:**753–760. http://dx.doi.org/10.1002/elps.200700782.
31. **Bose M, Whittal RM, Miller WL, Bose HS.** 2008. Steroidogenic activity of StAR requires contact with mitochondrial VDAC1 and phosphate carrier protein. J Biol Chem **283:**8837–8845. http://dx.doi.org/10.1074/jbc.M709221200.
32. **Bose HS.** 2011. Mechanistic sequence of mitochondrial cholesterol transport by StAR proteins. J Proteins Proteom **2:**1–9.
33. **Pawlak KJ, Prasad M, McKenzie KA, Wiebe JP, Gairola CG, Whittal RM, Bose HS.** 2011. Decreased cytochrome c oxidase IV expression reduces steroidogenesis. J Pharmacol Exp Ther **338:**598–604. http://dx.doi.org/10.1124/jpet.111.182634.
34. **Rosenfeld J, Capdeville J, Guillemot JC, Ferrara P.** 1992. In-gel digestion of proteins for internal sequence analysis after one- or two-dimensional electrophoresis. Anal Biochem **203:**173–179. http://dx.doi.org/10.1016/0003-2697(92)90061-B.
35. **Mukhopadhyay A, Heard T, Wen X, Hammen P, Weiner H.** 2003. Location of the actual signal in the negatively charged leader sequence involved in the import into mitochondrial matrix space. J Biol Chem **278:**13712–13718. http://dx.doi.org/10.1074/jbc.M212743200.
36. **Chuck S, Lingappa V.** 1992. Apolipoprotein B intermediates. Nature **355:**115–116. http://dx.doi.org/10.1038/355115a0.
37. **Schatz G, Dobberstein B.** 1996. Common principles of protein translocation across membranes. Science **271:**1519–1526. http://dx.doi.org/10.1126/science.271.5255.1519.
38. **Clark BJ, Wells J, King SR, Stocco DM.** 1994. The purification, cloning and expression of a novel luteinizing hormone-induced mitochondrial protein in MA-10 mouse Leydig tumor cells. Characterization of the steroidogenic acute regulatory protein (StAR). J Biol Chem **269:**28314–28322.
39. **Hegde RS, Mastrianni JA, Scott MR, DeFea KA, Tremblay P, Torchia M, DeArmond SJ, Prusiner SB, Lingappa VR.** 1998. A transmembrane form of the prion protein in neurodegenerative disease. Science **279:**827–834.
40. **von Heijne G.** 1986. Mitochondrial targeting sequences may form amphiphilic helices. EMBO J **5:**1335–1342.
41. **Harikrishna JA, Black SM, Szklarz GD, Miller WL.** 1993. Construction and function of fusion enzymes of the human cytochrome P450scc system. DNA Cell Biol **12:**371–379. http://dx.doi.org/10.1089/dna.1993.12.371.
42. **Rajapaksha M, Prasad M, Thomas JL, Whittal RM, Bose HS.** 2013. 3-Beta hydroxysteroid dehydrogenase2 (3βHSD2) requires chaperone-assisted folding for steroidogenic activity. ACS Chem Biol **8:**1000–1008. http://dx.doi.org/10.1021/cb400052s.
43. **Rajapaksha M, Thomas JL, Streeter M, Prasad M, Whittal RM, Bell JD, Bose HS.** 2011. Lipid-mediated unfolding of 3-beta hydroxysteroid dehydrogenase2 is essential for steroidogenic activity. Biochemistry **50:**11015–11024. http://dx.doi.org/10.1021/bi2016102.
44. **Lightowlers R, Chrzanowska-Lightowlers Z, Marusich M, Capaldi RA.** 1991. Subunit function in eukaryote cytochrome c oxidase. A mutation in the nuclear coded subunit IV allows assembly but alters the function and stability of yeast cytochrome c oxidase. J Biol Chem **266:**7688–7693.
45. **Tandon S, Horowitz P.** 1986. Detergent-assisted refolding of guanidinum chloride-denatured rhodanese. J Biol Chem **261:**15615–15618.
46. **Jewett AI, Shea JE.** 2006. Folding on the chaperone: yield enhancement through loose binding. J Mol Biol **363:**945–957. http://dx.doi.org/10.1016/j.jmb.2006.08.040.
47. **Court D, Narang FE, Steiner H, Hodges RS, Neupert W, Lill R.** 1996. Role of the intermembrane-space domain of the preprotein receptor Tom22 in protein import into mitochondria. Mol Cell Biol **16:**4035–4042. http://dx.doi.org/10.1128/MCB.16.8.4035.
48. **De Paul AL, Mukdsi JH, Petiti JP, Gutierrez S, Quintar AA, Maldonado C, Torres A.** 2012. Immunoelectron microscopy: a reliable tool for the analysis of cellular processes. *In* Dehghani H (ed), Applications of immunocytochemistry. InTech, Rijecka, Croatia.
49. **Prasad M, Kaur J, Pawlak KJ, Bose M, Whittal RM, Bose HS.** 2015. Mitochondria-associated ER membrane regulates steroidogenic activity via StAR-VDAC2 interaction. J Biol Chem **290:**2604–2616. http://dx.doi.org/10.1074/jbc.M114.605808.
50. **Rimmer KA, Foo JH, Ng A, Petrie EJ, Shilling PJ, Perry AJ, Mertens HD, Lithgow T, Mulhern TD, Gooley PR.** 2011. Recognition of mitochondrial targeting sequences by the import receptors Tom20 and Tom22. J Mol Biol **405:**804–818. http://dx.doi.org/10.1016/j.jmb.2010.11.017.
51. **Nakai M, Endo T.** 1995. Identification of yeast MAS17 encoding the functional counterpart of mitochondrial receptor complex protein MOM22 of Neurospora crassa. FEBS Lett **357:**202–206. http://dx.doi.org/10.1016/0014-5793(94)01362-5.
52. **Abe Y, Shodai T, Mutu T, Mihara K, Toril H, Nishikawa SC, Endo T, Kohda T.** 2000. Structural basis of presequence recognition by the mitochondrial import receptor Tom20. Cell **100:**551–560. http://dx.doi.org/10.1016/S0092-8674(00)80691-1.
53. **Saitoh T, Igura M, Obita T, Ose T, Kojima R, Maenaka K, Endo T, Kohda D.** 2007. Tom20 recognizes mitochondrial presequences through dynamic equilibrium among multiple bound states. EMBO J **26:**4777–4787. http://dx.doi.org/10.1038/sj.emboj.7601888.
54. **Yamano K, Yatsukawa Y, Esaki M, Hobbs AE, Jensen RE, Endo T.** 2008. Tom20 and Tom22 share the common signal recognition pathway in mitochondrial protein import. J Biol Chem **283:**3799–3807. http://dx.doi.org/10.1074/jbc.M708339200.
55. **Shiota T, Mabuchi H, Tanaka-Yamano S, Yamano K, Endo T.** 2011. In vivo protein-interaction mapping of a mitochondrial translocator protein Tom22 at work. Proc Natl Acad Sci U S A **108:**15179–15183. http://dx.doi.org/10.1073/pnas.1105921108.
56. **Prasad M, Thomas JL, Whittal RM, Bose HS.** 2012. Mitochondrial 3-beta hydroxysteroid dehydrogenase enzyme activity requires a reversible pH-dependent conformational change at the intermembrane space. J Biol Chem **287:**9534–9546. http://dx.doi.org/10.1074/jbc.M111.333278.